

SKB R-23-15

ISSN 1402-3091

ID 2054266

April 2025

Contact modelling approach to simulate water flow in a rock fracture under normal loading – Modelling report of Task 10.2.2

Task 10 of SKB Task Force GWFTS – Validation approaches for groundwater flow and transport modelling with discrete features

Sami Naumer, Veli-Matti Pulkkanen
VTT Technical Research Centre of Finland Ltd

Keywords: Water flow, Contact modelling, Numerical modelling, Blind prediction, Validation, COMSOL Multiphysics, Rock fracture, Fracture surface

This report concerns a study which was conducted for Svensk Kärnbränslehantering AB (SKB). The conclusions and viewpoints presented in the report are those of the authors. SKB may draw modified conclusions, based on additional literature sources and/or expert opinions.

This report is published on www.skb.se

© 2025 Svensk Kärnbränslehantering AB

Abstract

This report is a part of SKB Task Force on Modelling of Groundwater Flow and Transport of Solutes and focuses on Task 10.2.2c. In the task, the objective was to predict flow rates in a natural fracture between two rock parts which were compressed together with different normal loads. In the experiment carried out within the POST project, the rock samples were prepared and the first hydro-mechanical tests were conducted while the rock fracture remained unopened. After the tests, the fracture was opened, and the fracture surfaces scanned with high-precision instruments. Further flow tests were performed in the same fracture after the rock parts were re-emplaced together.

Using the fracture surface scan data and information on the placement of the rock parts in the experiment, different modelling teams conducted the blind prediction exercise where the flow rates under different normal loads were predicted. The experimental flow rate results were only provided after the predictions had been made. Our modelling team selected a modelling approach, where the rock-mechanical deformation was simulated with contact modelling followed by fluid flow modelling in the deformed fracture void space. Both the contact and fluid flow numerical modelling were conducted with COMSOL Multiphysics.

Preliminary analytical and numerical models were created to better understand the model uncertainties including fracture scan precision and placement of the top fracture surface with respect to the bottom one. These preliminary models showed that the scan precision is important when modelling slow flow, and that the fracture surface placement deviations especially in z- but also x- and y-directions are statistically significant factors affecting the flow rate.

The preliminary models were followed by converting the experimental fracture surface scan data into a model geometry which consists of the two rock parts separated by the fracture. The rock parts were virtually compressed against each other, and the contact of the fracture surfaces and the deformation of the linear elastic assumed rock were simulated with two different approaches, Nearing Contact Model and Departing Contact Model. With the first model, a normal load of 1 MPa was considered while with the latter normal loads of 0, 1, 2, 4, 6 and 8 MPa were studied. Even though the contact formulations aimed to prevent geometrical overlap of the fracture surfaces, this was not achieved perfectly. Thus, a contact offset value was used in the contact modelling to prevent the overlap, which was important for the subsequent flow modelling. The contact offset, however, added error to fracture geometry and, therefore, to the flow model, and a balance between modelling error and preventing the overlap had to be sought.

The resulting stress distribution from both contact modelling approaches showed that the uniaxial compressive strength was exceeded in some areas on the surfaces and possible breaking of the rock could occur. This indicates that the assumption of linear elastic deformation induced uncertainty to the model. On the other hand, the simulated displacements between the top and bottom rock parts showed a somewhat similar trend with high normal loads (over 2 MPa) as the measured LVDT data, which gives some confidence in the only elastic model.

The deformed fracture void space between the two rock parts that resulted from the contact modelling was converted into a flow channel geometry where the water flow driven by pressure difference was simulated. Very slow flow rate was assumed, leading to the use of the Navier-Stokes equations without the inertial term. The predicted flow rates significantly overestimated the experimentally measured flow rate with both approaches and with the different normal loads. The flow rates also varied depending on the contact approach and the contact offset value.

The main sources of uncertainties in the simulations were considered to be 1) the used contact offset, 2) the fracture surface scan precision, 3) the initial placement and the overlap of the fracture surfaces resulting from the surface scan data and position measurements, 4) the numerical error especially in fracture surface interpolation, and 5) the linear elastic assumption of rock mechanical behaviour. The difference in the modelled and measured flow rates was, however, so large that it could not be explained by these sources of uncertainties. This suggests that an unknown, highly influential factor is missing from the modelling.

A validation rank approach was suggested to complement the pragmatic validation approach by the Task Force. The initial test to apply the approach to the modelling in this report indicates that the approach should be further tested for other modelling and likely improved at least in the details.

Sammanfattning

Denna rapport är en del av arbetet inom SKB Task Force GWFTS för modellering av grundvattenflöde och transport av lösta ämnen och fokuserar på Modelleringsuppgift 10.2.2c. I uppgiften var syftet att prediktera flödes hastigheter i en naturlig spricka mellan två bergdelar som trycktes ihop med olika belastningar i normalriktningen. I experimentet som genomfördes inom POST-projektet preparerades bergproverna och de första hydromekaniska testerna genomfördes medan bergsprickan förblev öppen. Efter testerna öppnades sprickan och sprickytorna skannades med ett högprecisionsinstrument. Ytterligare flödestester utfördes i samma spricka efter att bergdelarna återplacerats tillsammans.

Med hjälp av skannade data från sprickytan och information om placeringen av bergdelarna i experimentet genomförde olika modelleringsteam denna övning i blind prediktering där flödes hastigheterna under olika belastningar i normalens riktning predikterades. De experimentella flödes hastighetsresultaten gavs först efter att prediktionerna hade gjorts. Vårt modelleringsteam valde en modelleringsmetod, där den bergmekaniska deformationen simulerades med kontaktmodellering följt av flödesmodellering i det deformerade sprickhållrummet. Både den numeriska kontakt- och flödesmodelleringen utfördes med COMSOL Multiphysics.

Preliminära analytiska och numeriska modeller skapades för att bättre förstå osäkerheter i modelleringen inklusive sprickskanningsprecision samt placeringen av den övre sprickytan i förhållande till den nedre. Dessa preliminära modeller visade att skanningsprecisionen är viktig vid modellering av långsamt flöde, och att sprickytplaceringsavvikelse särskilt i z- men även x- och y- riktningar är statistiskt signifikanta faktorer som påverkar flödes hastigheten.

De preliminära modellerna utvecklades genom att omvandla den experimentella sprickytnas skanningsdata till en modellgeometri som består av de två bergdelarna som är åtskilda av sprickan. Bergdelarna var praktiskt taget hoptryckta mot varandra, och sprickytnas kontakt och deformationen av det linjärt elastiska antagna berget simulerades med två olika tillvägagångssätt, "Nearing Contact Model" och "Departing Contact Model". Med den förstnämnda modellen användes en belastning på 1 MPa emedan den andra modellen användes för att studera belastningar på 0, 1, 2, 4, 6 och 8 MPa i normalriktningen. Även om formuleringarna av kontaktytan syftade till att förhindra geometrisk överlappning av sprickytorna, uppnåddes detta inte perfekt. Därför användes ett kontakt-offsetvärde i kontaktmodelleringen för att förhindra överlappningen, vilket var viktigt för den efterföljande flödesmodelleringen. Kontaktförskjutningen orsakade dock fel till sprickgeometrin och därför även till flödesmodellen, så det gällde att hitta en balans mellan modelleringsfel och förhindrande av överlappningen.

Den resulterande spänningsfördelningen från båda kontaktmodelleringssätten påvisade att den enaxliga tryckhållfastheten överskreds i vissa områden på ytorna så att brott på sprickytorna kunde eventuellt inträffa. Detta indikerar att antagandet om linjär elastisk deformation inducerade en osäkerhet i modellen. Å andra sidan påvisade de simulerade förskjutningarna mellan de övre och nedre bergdelarna en liknande trend vid höga normallaster (över 2 MPa) som de uppmätta LVDT-data, vilket ger en viss tilltro till den elastiska modellen.

Det deformerade sprickhållrummet mellan de två bergdelarna som blev resultatet av kontaktmodelleringen omvandlades till en flödeskanalgeometri där det simulerade vattenflödet drivs av en tryckskillnad. En mycket långsam flödes hastighet antogs, vilket ledde till användningen av Navier-Stokes ekvationer utan tröghetstermen. De predikterade flödes hastigheterna överskattade signifikant de experimentellt uppmätta flödes hastigheterna vid användande av båda tillvägagångssätten för de olika normalbelastningarna. Flödes hastigheterna varierade också beroende på kontaktmetoden och kontaktoffsetvärdet.

De huvudsakliga källorna till osäkerheter i simuleringarna ansågs vara 1) den använda kontaktförskjutningen, 2) sprickytans skanningsprecision, 3) den initiala placeringen och överlappningen av sprickyterna till följd av sprickytskanningsdata och positionsmätningar, 4) det numeriska felet speciellt vid sprickyteinterpolation, och 5) det linjära bergmekaniska egenskaperna hos berget. Skillnaden i de modellerade och uppmätta flödes hastigheterna var dock så stor att den inte kunde förklaras av dessa osäkerhetskällor. Detta tyder på att en okänd, mycket inflytelserik faktor saknas i modelleringen.

Ett annat tillvägagångssätt för validering, som inkluderar rankning, föreslogs för att komplettera den pragmatiska valideringsmetoden som används av Task Force GWFTS. Det första testet av att tillämpa tillvägagångssättet på modelleringen i denna rapport indikerar att tillvägagångssättet bör testas ytterligare för användning i annan modellering och sannolikt behöver detaljerna förbättras.

Acknowledgements

We would like to acknowledge Posiva for funding this research. We would like to thank the task evaluator Dr. Stefan Finsterle for valuable comments that improved the report significantly. We would also like to thank the Task Force and the other modelling groups who provided valuable insights and feedback that helped to shape our research.

Content

Acknowledgements	5
Abbreviations	7
1 Introduction	8
2 Description and objectives of Task 10.2.2	9
2.1 Objectives of Task 10.2.2.....	9
2.2 Limitation of Task 10.2.2	9
2.3 Data description.....	10
2.4 Pragmatic validation.....	11
3 Modelling and methodology	13
3.1 Modelling tasks	13
3.1.1 Model purpose.....	13
3.1.2 Model description.....	14
3.1.3 Determination of critical aspects.....	26
3.1.4 Model parameters	26
3.1.5 Identification of influential factors	28
3.1.6 Uncertainty analyses.....	29
3.1.7 Workflow describing the modelling process.....	30
3.1.8 Pragmatic validation aspects	32
4 Results	33
4.1 Analytical Model.....	33
4.2 Contact models.....	37
4.2.1 Nearing Contact Model	37
4.2.2 Departing Contact Model	40
4.3 Experimental results and inverse calculations.....	46
5 Discussion and conclusions	48
5.1 Discussion	48
5.1.1 Analytical solution	48
5.1.2 Parallel Plate Model	48
5.1.3 Small Surface Model.....	48
5.1.4 Contact models.....	49
5.1.5 Discussion of the modelling goals.....	55
5.1.6 Other discussion	56
5.1.7 Pragmatic validation.....	57
5.2 Conclusions	58
References	60
Appendix A	61

Abbreviations

Design of experiments	DoE
Definitive Screening Design	DSD
Uniaxial compressive strength	UCS
Navier–Stokes	NS

1 Introduction

The modelling effort described in this report is a part of Task 10 by SKB Task Force on Modelling of Groundwater Flow and Transport of Solutes. Multiple modelling teams, our modelling team included, aimed to develop modelling approaches that can be used to validate models of water flow in rock fractures. The specific topics of interest are the development of pragmatic validation approaches and the channelling of the flow. Throughout Task 10, fracture flow modelling is scaled up from a single fracture scale to larger scales up to a deposition hole scale. The different modelling teams can use different approaches in model creation and focus on different aspects of fracture flow.

Within Task 10.2.2 for single fracture flow, our modelling team focused on Task 10.2.2c defined by the Task Description (Bruines, unpublished, which will be denoted solely Task Description in the following of this report)¹, in which the objective was to understand how different normal loads perpendicular to a single rock fracture affect flow in it. For the flow experiment to be modelled in the subtask, a rock sample with a natural fracture was identified, and a laboratory-scale sample was cut from it. The outer geometry of the sample was measured with high-resolution devices. Flow rates through the fracture were measured while the normal load was varied. The rock sample separated by the natural fracture was split open after the flow tests. The fracture surfaces were then also measured to create a high-resolution dataset of the fracture geometry (Jacobsson and Godio 2023, Godio and Jacobsson, 2024). Another set of hydromechanical tests was performed after the fracture had been split, measured and put back together.

The overall objective of the modelling teams was to come up with ways of predicting fluid flow in the fracture under different loads using the high-resolution fracture geometry data, rock parts placement data and provided boundary conditions, such as pressure at the inlet and outlet. With this, the hydromechanically coupled behaviour occurring in the fracture should be better understood. To allow blind predictions of the flow rates, the subtask was carried out such that the results of the hydromechanical tests were not published to the modelling teams initially. The teams were also supposed to study how the fluid is channelled as it flows through the rough fracture.

Our modelling group's overall approach was to model the deformation of the fracture under different normal stresses, and afterwards model the fluid flow within the deformed void space. Based on the provided data, our modelling group selected fracture surface contact modelling as an approach for the deformation modelling. Very slow flow in the deformed fracture was assumed and, consequently, Navier-Stokes equations without the inertial term were used when modelling the flow. The effect of the water pressure on the upper rock part was omitted.

For the numerical modelling, COMSOL Multiphysics (COMSOL, 2022a) was selected as the modelling tool. The software is a finite-element method tool widely used in numerical modelling of problems where multiple different physics are coupled. For Task 10.2.2c it allowed for a continuous workflow, where the provided fracture scan data is imported and generated into a geometry followed by both contact and fluid flow modelling. If needed, the workflow can be fully automated which would enable sensitivity analysis on any of the steps involved.

The simulation results and back analysis of the experimental results (after they were revealed) were used to analyse whether sensible predictions of fluid flow can be obtained with the approach considering all the unavoidable limitations to the model (presented in Section 2.2). Prior to modelling deformation of the void space, uncertainties regarding model resolution and fracture surface placement, among others, were also studied.

¹ Bruines, P. SKB Task Force on Modelling of Groundwater Flow and Transport of Solutes: Description of Task 10.2. SKB R-23-10, Svensk Kärnbränslehantering AB, Stockholm, Sweden. Unpublished.

2 Description and objectives of Task 10.2.2

2.1 Objectives of Task 10.2.2

The Task Description defines the objectives of Task 10.2.2 as 1) prediction and validation of the upscaled fracture geometry from borehole sized fracture geometry and/or fracture trace geometry, 2) prediction and validation of flow along a fracture at different normal stresses, and 3) support of the development and demonstration of pragmatic validation workflow at the single fracture scale.

Our modelling team focused on Subtask 10.2.2c: “Prediction-outcome exercise of flow along an unopened fracture at different normal loads”, for which the second and third objective are applicable. The specific objectives of our modelling group are:

- 1) Understanding the effect of measurement precision and fracture surface placement uncertainties on fracture flow by prior (to flow experiments) sensitivity analysis and by simple inverse modelling of the experimental results using the cubic law for an assumed flat-plate fracture.
- 2) Predicting the fracture flow rate of the POST experiment for different normal loads and contributing to the understanding of flow channelling with a model that mimics the fracture surfaces mechanical contact and that simulates three-dimensional fluid flow between the fracture surfaces.
- 3) Analysing the validity of the created contact- and fluid flow model by using the outcomes of the fluid flow experiment and the predictive simulations.

2.2 Limitation of Task 10.2.2

According to the Task Description, the overall objective of Task 10 is “... to develop pragmatic approaches to model validation within the Task Force”. The first modelling task, Task 10.2, “focuses on flow and transport at the single fracture scale, with emphasis on in-fracture channelling”. The experimental setup that is used for the prediction-outcome exercise of flow along an unopened fracture at different normal loads (Task 10.2.2c) does not provide information on flow channelling, and, therefore, the models for the emphasized feature of in-fracture channelling cannot be validated with the aimed validation approach.

Subtask 10.2.2c does not include a separate model development or model conditioning (to experimental information) phase. This implies that the current understanding of single fracture flow is that it is possible to model water flow in a fracture only with information on fracture surface geometries, with measurement data of the top and bottom fracture surface positions with respect to each other, with measurements of the rock block outer surface positions, and with basic mechanical material parameters. Consequently, the validation process in the subtask focuses on validating this understanding.

The overall limitations identified in the Task Description are the uncertainties related to the rock fracture stress, thermal and geochemical evolutions, which vary between fractures of different origins. The fracture used for the hydromechanical coupled flow represent only one specific fracture type (clean fracture in shallow depth with limited mineral precipitation).

The provided experimental data contained some inherit limitations. The precision of the fracture surface scan device was 0.035 mm. This means that two points closer to each other than the precision cannot be distinguished from each other reliably. Consequently, apertures smaller than the precision are not accurately captured by the measurement, which could affect the flow modelling. Furthermore, the point resolution in the point cloud created by the fracture scans was 0.1 – 0.2 mm. Thus, surface undulations and unevenness on a smaller scale are omitted from the models.

Apart from the fracture scans, the rate of outflowing water in the experiment could affect the measurement precision. If flow rates are very small, it is difficult to measure the rate accurately.

Opening of the fracture might have caused permanent deformation of the rock close to the fracture surfaces. When the rock pieces are again placed together, the deformed areas might re-deform such that the measured fracture surfaces do not match the surface geometries of the fractures placed on top of each other. This phenomenon is difficult to capture with modelling without somehow measuring it, which is likely also difficult.

2.3 Data description

The Task Description describes the different types of data. In this section we have summarised the data we have utilized in our modelling and, also, pointed out data that was not used.

The geometrical data of the unopened rock sample includes measurements of the outer surfaces of the sample. Such measurements could be compared with data of the reassembled rock sample to, for example, study how much the sample has permanently deformed in the process. However, as our modelling team omits permanent deformations in the models at this point, the detailed data was not used.

The provided Linear Variable Displacement Transducer (LVDT) data of the movement of the upper rock part in relation to the lower one was used for comparison with the mechanical contact model predictions.

The measured rock sample outer dimensions of 200 x 200 x 250 mm were used in creation of the model geometry. Furthermore, the measurements of the opened fracture surfaces were the primary data used in the model generation. This data included x-, y-, and z-coordinates of measurement points that were obtained with laser scans. We used the data set where the provided data points were connected with line segments to create a triangular surface mesh that represents the fracture surface geometry. The mesh had a total of 4,121,453 points on the bottom surface and 3,924,543 points on the top surface. The fracture surface geometry was further processed for the simulations, meaning that the simulation mesh differs from the surface mesh according to the measurements.

We also used the surface scan data from smaller rock samples (from Task 10.2.1) to evaluate the uncertainties related to the top and bottom rock part placements when put on top of each other.

In addition to the point-cloud and triangulated fracture surface data, high-resolution photographs of the rock sample were provided. They were not used in our modelling approach. Furthermore, the provided LVDT-displacement data is not used for creating the deformed rock part geometries. It can, however, be used in comparing the resulting displacements to the observed ones.

In the contact model, the provided intact rock parameters, including the Young's modulus and the Poisson's ratio, were used to describe elastic deformation of the rock sample in the contact model. In addition, a uniaxial compressive strength (UCS) was provided. Although no permanent deformation was modelled, the UCS was used to estimate in which areas of the fracture surfaces permanent deformation could occur based on the resulting stress state in the contact model (if von Mises stress is higher than the measured UCS). The contact pressure measurements were also used to compare whether the contact in the model and in the experiment are located in similar areas.

For the flow test, properties of water, including inlet and outlet pressure, and temperature, were provided in the Task Description. The detailed, time-varying data for either was not used at this stage of modelling and instead average values were utilized. These values define the head gradient and viscosity in the fluid flow problem, discussed later in Section 3.1.4. After the modelling groups had provided their predictions of flow rates, the experimental results corresponding to different normal loads were given. These were used in the prediction-outcome exercise for pragmatic model validation.

2.4 Pragmatic validation

In Task 10, the definition of validation stated by IAEA (2019) is used: “Model Validation: The process of determining whether a model is an adequate representation of the real system being modelled, by comparing the predictions of the model with observations of the real system.”

According to the view taken by the Task Force (Lanyon et al., 2021), the modelling approaches and workflows should be validated to a specific, intended purpose. Although the intended purpose can range from understanding the basic phenomena (with detailed, small scale models) to estimating the release of radionuclides from a spent nuclear fuel repository (with a disposal site scale model), it is anticipated that the approach may lead to scatter in modelling approaches when implemented by the modellers focusing on specific modelling tasks (a different, often detail focused modelling approach for each modelling task with a different purpose). Without measures to link the models to one another (different in phenomena, scale and complexity) or to merge the information, the scatter could lead to reduced confidence in models, which is opposite to the intend of the validation process. For example, if there are several phenomena that groundwater flow models for spent nuclear fuel repositories are expected to be able to predict (say, water inflow into an empty borehole, connectivity of flow network on repository scale, and advective transport of radionuclides) and the phenomena are explained by separate validated-for-a-purpose models which are based on completely different conceptual models (say, an equivalent porosity model, a discrete fracture network model and a channel model) and there is no attempt to link them to each other, the evaluator of the models might ask: “Why do you need this many different models to explain the basic phenomena?”

Similarly, the modellers often focus on tasks that include separate, non-coupled processes with a process specific purpose (or processes with a few couplings). The process could be, for example, rock deformation with associated purpose to evaluate the mechanical load on disposal barriers, or reactive transport with purpose of evaluating radionuclide sorption in detail. If these models are not linked to other models describing the same material or site, a risk for model and information scatter exists.

If the pragmatic validation approach towards general objectives (such as understanding flow channelling from single fracture to repository scale) is implemented using only general instructions on the overall validation process and the modellers should provide only qualitative descriptions of the validation (in specific modelling tasks) without metrics to evaluate the general process, the validation may become of secondary interest for the contributors. To encourage linking models with different phenomena and in different scales to each other and to try to avoid knowledge and model divergence, a validity rank approach was developed and is suggested for model validity evaluation. According to the approach, the model “validity” depends on the number of single validation-for-a-single-phenomenon exercises it has passed and on the number of different phenomena it can explain. To this end, the validity rank R of a model defined as

$$R = n \cdot m^{(1+p)} \quad (1)$$

is suggested. Here, m is the number of phenomena or combinations of the phenomena that the model has been validated for, n is the number of validation-for-a-single-phenomenon exercises it has passed, and p is the number of coupled validation exercises it has passed. Aiming to increase the validation rank would encourage model development towards convergent models that could be used to explain several experimental observations with a single, consistent model. It would also encourage the modellers to proceed with model development only when the model can be validated.

Let us take a few examples of the validity rank.

Example 1. A model that can explain connectivity of a flow network and has been validated for that purpose has a rank of $1 \cdot 1^{(1+0)} = 1$.

Example 2. If a model that can explain connectivity of a flow network and also flow into an empty borehole has been validated for those phenomena separately, it has a validity rank of $2 \cdot 2^{(1+0)} = 4$. If the same model has been additionally validated for both phenomena simultaneously, the validity rank would be $2 \cdot 2^{(1+1)} = 8$.

Example 3. A model that has hydraulic and mechanical components, each of which has been validated separately twice, would have a rank of $4 \cdot 2^{(1+0)} = 8$. If the model has been additionally validated for both phenomena simultaneously with two separate validation exercises, it would have a validity rank $4 \cdot 2^{(1+2)} = 32$.

Example 4. A model that has hydraulic, mechanical and chemical components, each of which has been validated separately, would have a validity rank of $3 \cdot 3^{(1+0)} = 9$. If the model has been additionally validated for all three phenomena simultaneously with two separate validation exercises, it would have a validity rank $3 \cdot 3^{(1+2)} = 81$.

It is acknowledged that defining a successful validation exercise or counting the numbers n, m and p may be somewhat arbitrary and subjective. It is also acknowledged that the approach could be further developed to better account for complex model couplings, and it should be tested in practise to see if it is pragmatic.

3 Modelling and methodology

3.1 Modelling tasks

Our modelling team modelled Task 10.2.2c: “Prediction-outcome exercise of flow along an unopened fracture at different normal loads”, in which, according to the Task Description, “Modellers are to:

- Develop a fracture void representation of the fracture in its unopened and unloaded state,
- Develop a mechanical model of the change of the fracture void space under different normal loads,
- Calculate the flow through the fracture at different normal loads and hydraulic heads,
- Compare modelled and measured flow rates, and optimise models where possible.”

This structure was followed with a series of modelling approaches to cover the objectives of this study. In this section, the modelling approach, specific objectives and validation aspects utilised by this modelling group are presented.

3.1.1 Model purpose

Five different models were utilized to pursue the model objectives described in Section 2.1. The models are 1) the Analytical Model, 2) the Parallel Plate Model, 3) the Small Surface Model, 4) the Nearing Contact Model, and 5) the Departing Contact Model.

In Section 3.1.2, it is described how a contact offset is required in the contact models to prevent geometrical overlap of the upper rock part to the lower one. The purpose of the Analytical Model is to give an estimation of the influence such an offset has on the total flow rate and how this can be compared with the surface scan precision of the fracture surfaces using the cubic law. An additional purpose of the Analytical Model is to help with the back analysis of the uncertainties in the experimental results and their meaning with respect to the detailed modelling.

The purpose of the Parallel Plate Model is to serve as a bridge between the Analytical Model and the subsequent models with detailed fracture surface geometries and mechanical contact. More specifically, it is a simple three-dimensional numerical model (with rectangular cuboid model geometry) used to ensure that the numerical implementation (chosen numerical methods together with mesh type and density as well as boundary conditions) is sufficient with respect to accuracy but computationally not too heavy for the next more demanding modelling steps. The Parallel Plate Model also helps in estimating the effect of fracture surface measurement precision on the numerical model simulation results.

The Small Surface Model is used to perform a sensitivity analysis to better understand how rigid displacement of the top fracture surface in relation to the lower one affects the flow rate. The surface scan data from Task 10.2.1 on smaller fractures were used for the fracture geometry. The results of the sensitivity analysis can be used to justify assumptions made for the contact models.

The purpose of the last two models, the Departing and Nearing Contact Models, is to simulate the deformation of the fracture surfaces under different normal loads and to predict the flow rates in the deformed void space. In addition, the purpose is to use the models to estimate the channelling of the fracture flow.

A secondary purpose of the entire workflow with the five different models is to develop and improve the contact modelling for the fracture surface compression to each other. As the amount of provided fracture surface point data is large and the surfaces themselves complex in shape, contact can be difficult to model. Thus, the model development can provide lessons learned on whether contact modelling is applicable for predicting the outcomes in fluid flow experiments such as the one defined by the Task Description.

3.1.2 Model description

First, the conceptualization of phenomena related to the flow experiment provided by the Task Description are described in this section. This is followed by a description of conceptual models for the different modelling approaches our modelling team utilized in representing the experimental setup numerically. The conceptual models help to understand the mathematical and numerical model later in this section.

Conceptual model

For Analytical and Parallel Plate Models, we assume stationary, fully developed, slow flow without inertial effects in the space between parallel smooth planes. The distance between the planes is called effective aperture to distinguish it from the pointwise aperture between undulating fracture surfaces.

For the Small fracture model, we assume similar flow as for the Analytical and Parallel Plate Models, but within a three-dimensional aperture formed between fracture surfaces that are reasonable accurate representations of the real fracture surfaces.

For the Contact models, we assume that the experiment of the Task Description can be described with two key processes. The first process is the normal compression of the rock blocks that makes them to deform, causing also the open fracture space between them to deform. The rock can either deform elastically, or permanently due to plastic processes or breaking of rock if the resulting stresses are higher than the yield limit or the ultimate strength of the rock. Initially, we assume elastic deformation; more complicated permanent deformations may be added to the model if the yield limit or strength are reached. In the case of an undulating fracture surface, deformation is expected especially in areas where the two surfaces are in contact. The smaller the contact area, the higher the resulting stresses and thus the larger the deformation. Increasing the normal load decreases the fracture void space which, in turn, decreases the flow rate. The effect of water pressure on the deformation of the rock was omitted (also in the unloaded, zero normal load case). The conceptual model is visualised in Figure 3-1.

The second process describes the fluid flow in the fracture void space between the upper and lower rock parts. We use a three-dimensional reasonably accurate representation of the deformed rock fracture where water can flow slowly (without inertial effects). We assume that the fracture is not filled with a filling material, such as clays or other minerals (Brady and Brown, 1985). In the beginning of the experiment, the openings can be either filled with air or water, but here we assume that the entire void space is fully water saturated. We also assume that the properties of the water are constant. Furthermore, the capillary action's effect on the flowrate was assumed to be negligible.

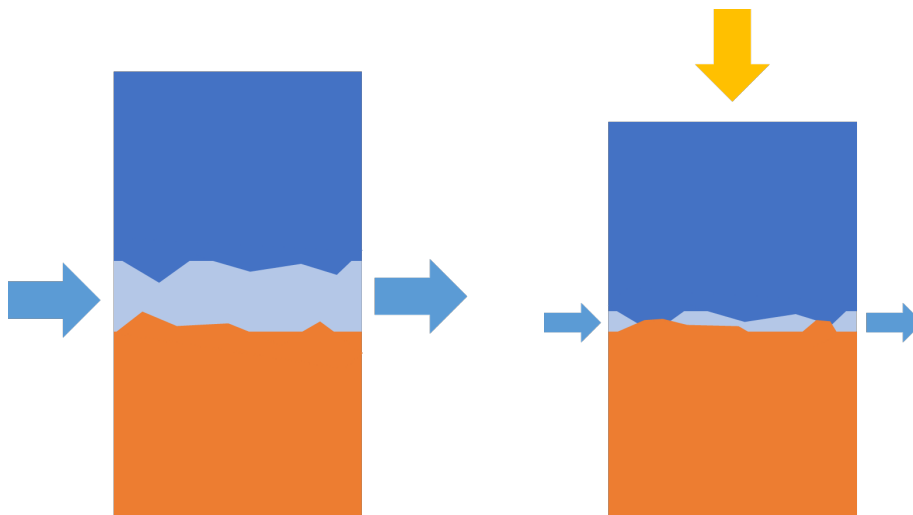


Figure 3-1. The conceptual model of the compression of rock blocks is illustrated graphically. The top rock part is blue and the bottom part orange. The void space between the rock parts is light blue. Water flows through the undeformed void space on the left. In this 2D illustration, the fracture is completely open, but in reality, there are contact points also in the unloaded case. On the right, the rock is compressed with a normal load (represented with the downwards pointing yellow arrow) and water flows through the deformed void space. The blue arrows represent flow rate.

Mathematical model

The mathematical model description focuses on the two main processes, the fluid flow in the void space and the deformation of the fracture space.

Motion of a viscous fluid is described by the Navier–Stokes (NS) equation

$$\rho \left(\frac{\partial \mathbf{v}}{\partial t} + \mathbf{v} \cdot \nabla \mathbf{v} \right) = -\nabla p + \mu \nabla^2 \mathbf{v} + \mathbf{F}, \quad (2)$$

where \mathbf{v} is the fluid velocity, t the time, p the pressure, μ the viscosity of the fluid, and \mathbf{F} the external forces, such as gravity. We assume that the fluid is incompressible. Thus,

$$\nabla \cdot \mathbf{v} = 0. \quad (3)$$

For the *Analytical Model*, fluid is assumed to flow between two parallel plates. The fluid flow is assumed Newtonian with a constant density and viscosity. The flow is assumed to be steady, the effect of inertia and gravity are omitted, and the flow velocity is zero at the walls of the flow channel. The setup is visualised in Figure 3-2.

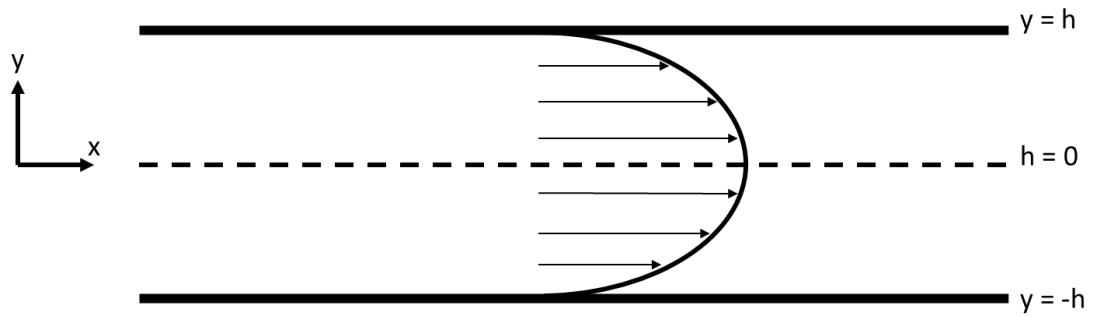


Figure 3-2. Visualisation of fluid flow between two parallel plates. The analytical solution is based on this setup.

With these assumptions, Equation (2) simplifies to x-directional velocity:

$$v_x = \frac{1}{2\mu} \left(\frac{\partial p}{\partial x} \right) (y^2 - h^2) \quad (4)$$

A scalar flow rate can then be calculated by integrating Equation (4) with $-h$ and h as the limits, taking the absolute value and by multiplying by the width of the flow channel (W). For the multiplication, it is assumed that the side walls of the flow channel have negligible effect on the fluid flow due to the ratio between the channel width and the aperture being large. This gives us:

$$Q = W \cdot \frac{d^3}{12\mu} \left| \frac{\partial p}{\partial x} \right|, \quad (5)$$

where Q is the flow rate and d the aperture of the flow channel. This equation, also called the cubic law, was later used to calculate flow rates corresponding to different apertures. The results of this are presented in Section 4.1.

For 3D flow, which is used in the numerical models, we also assume that the fluid is Newtonian with a constant density and viscosity. The flow is assumed to be steady, the effect of gravity is omitted. The flow is also assumed to have a very low Reynolds number and the inertial forces are negligible. It is also assumed that all fluid flows in the flow channel and no flow occurs within the rock domain. Thus, the Navier-Stokes equations (2-3) reduce to the Stokes equation that is solved in the 3D case:

$$-\nabla p + \mu \nabla^2 \mathbf{v} = 0, \quad (6)$$

where ∇p is the pressure gradient, μ the viscosity of the fluid, and \mathbf{v} the velocity of the fluid.

The rock that surrounds the fracture void space is assumed to be homogenous and continuous without any fractures or defects apart from the fracture separating the rock parts. The rock material is also assumed to be linear elastic and isotropic and the effect of gravity is omitted. The equation of motion in a stationary case can then be expressed as

$$\nabla \cdot \boldsymbol{\sigma} = 0 \quad (7)$$

and the linear elastic constitutive law is

$$\boldsymbol{\sigma} = \frac{E}{(1 + \nu)} \left[\boldsymbol{\varepsilon} + \frac{\nu}{(1 + 2\nu)} \text{tr} \boldsymbol{\varepsilon} \mathbf{I} \right] \quad (8)$$

where $\boldsymbol{\sigma}$ is stress tensor, E is the Young's modulus, ν is the Poisson's ratio, $\boldsymbol{\varepsilon} = 1/2(\nabla \mathbf{u} + \nabla \mathbf{u}^T + \nabla \mathbf{u}^T \nabla \mathbf{u})$ the strain tensor with \mathbf{u} the displacement, tr the trace operator and \mathbf{I} the identity tensor.

Numerical models

Predictions of flow rates in a simple geometry are possible with the analytical solution. However, already in the 3D case of flow between parallel plates, analytical solutions are much more complicated and with a detailed fracture geometry virtually impossible to find. Thus, numerical methods were utilised. In this study our modelling team selected COMSOL Multiphysics as the software used for the numerical modelling. The software allows implementing the desired conceptual models for both contact and fluid flow modelling within a single software and the modelling team has prior experience with the software. This simplifies the modelling workflow and enables full automation of the process, for example for a sensitivity analysis, which was performed using the *Small Surface Model*.

In this section the numerical models created in this study are explained. The first numerical model was the *Parallel Plate Model* where fluid flows between two parallel flat plates in three dimensions. The purpose of that model was to compare the analytical solution to a similar case in 3D using the experimental sample dimensions for the aperture. In addition, the model provides information on the needed mesh density for the subsequent numerical models. The second numerical model, the *Small Surface Model*, used detailed fracture surfaces from the previous Task 10.2.1 in a sensitivity analysis to better understand deviations in the upper fracture surface placement. The two final numerical models, the *Departing* and *Nearing Contact Models*, were the contact models, where the experimental setup was numerically replicated. In the models, rock deformation was simulated and flow rates in the deformed void space predicted. The two contact models used different contact modelling approaches described in detail in their respective sections.

Parallel Plate Model

In the first model, a three-dimensional model geometry with the width and length of 200 mm, and an effective aperture was created. This is based on the dimensions of the rock sample from the Task Description. However, instead of detailed fracture geometry, the top and bottom surfaces were flat as in the *Analytical Model*. The height of the geometry which represents fracture effective aperture was varied. A geometry with an effective aperture of 0.035 mm is presented in Figure 3-3. The effective apertures were varied between 0.01 mm to 0.10 mm. The effective aperture selection was based on the experimental fracture surface measurement precision so that both larger and smaller values were analysed. Material properties of water were assigned to the model geometry, with parameters presented in Section 3.1.4.

In addition to Equation (6), boundary conditions for the model must be defined. First, on the top, bottom and two opposing side walls, a no-slip condition is defined:

$$\mathbf{u} = 0. \quad (9)$$

Additionally, pressures corresponding to the average values used in the experiment of the Task Description were applied to the inlet and outlet of the geometry. The used properties are also presented in Section 3.1.4.

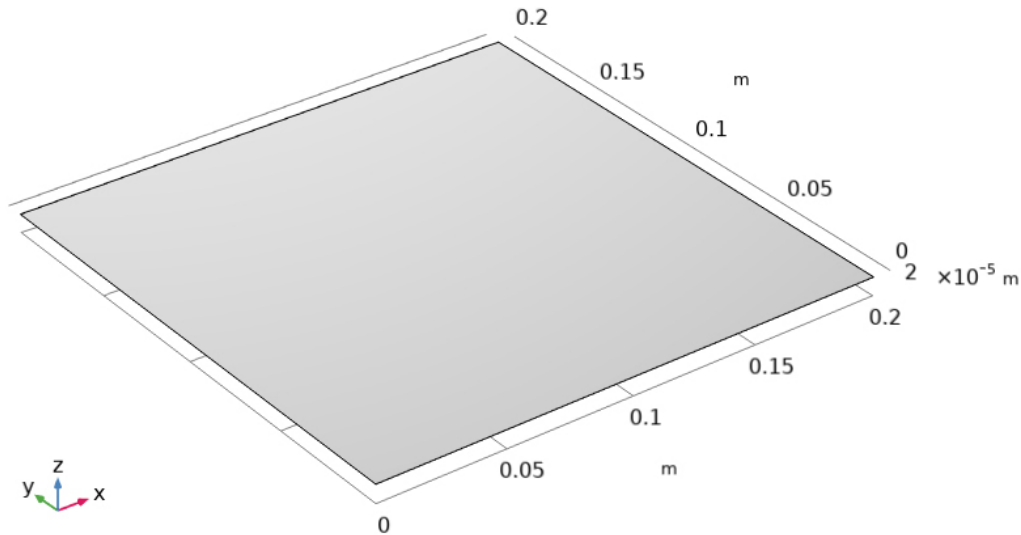


Figure 3-3. Geometry used in the Parallel Plate Model. Note that the height of the block is 0.035 mm.

A mesh was created with a free triangular mesh both on top and bottom surfaces of the model geometry. A minimum element size of 0.15 mm and a maximum size of 0.3 mm were used. This mesh was swept from top to bottom creating three layers of triangular prisms. The complete mesh consists of 3,204,558 domain elements and 2,144,376 boundary elements.

In COMSOL Multiphysics, a fully coupled nonlinear solver with a damped Newton's method with adaptive damping factor was used. PARADISO (COMSOL, 2022a) was used as the linear solver.

Small Surface Model

The mathematical formulation of the *Small Surface Model* is identical to that of the *Parallel Plate Model*. However, instead of flat fracture surfaces, realistic fracture surface geometries were used. The aim of the model was to create a sensitivity analysis on how the rigid displacements of the rock blocks (the shape or the size of the blocks does not change) affect the flow. The types of rigid displacements were the translation of the entire upper surface in x-, y-, and z-directions and rotation around the z-axis. The details of the sensitivity analysis are presented in Section 3.1.6.

As this model was created in early phases of the work, the scanned data for Task 10.2.2 of the Task Description was not available yet. Thus, the fracture data from Task 10.2.1 was used instead. 1N1-CLC-N and 1N1-CLC-U were used as the top and bottom fracture surfaces. The provided triangulated data of each surface was imported to COMSOL Multiphysics as such.

Cubic spline parametric surfaces were fitted to the data for both the upper and lower fracture surfaces. The cubic spline surfaces are continuous piecewise third order polynomial surfaces, which are defined using knot points (Bartels et al., 1998). The number of knots in the models was 200.

Creation of the parametric surfaces leads to a loss of point resolution and is one limitation of all models in this study, where the fracture surface data has been used. The surface dimensions were 70 mm in the x-direction and 100 mm in the y-direction. A part of the interpolated surface along with the original data points is visualised in Figure 3-4. As can be seen, the interpolation is accurate in areas where the original data was smooth. At the same time in areas where the original data was uneven, the interpolation smoothens the original data. This smoothing was noted when selecting an interpolation method and its effects were planned to be further studied in a sensitivity analysis.

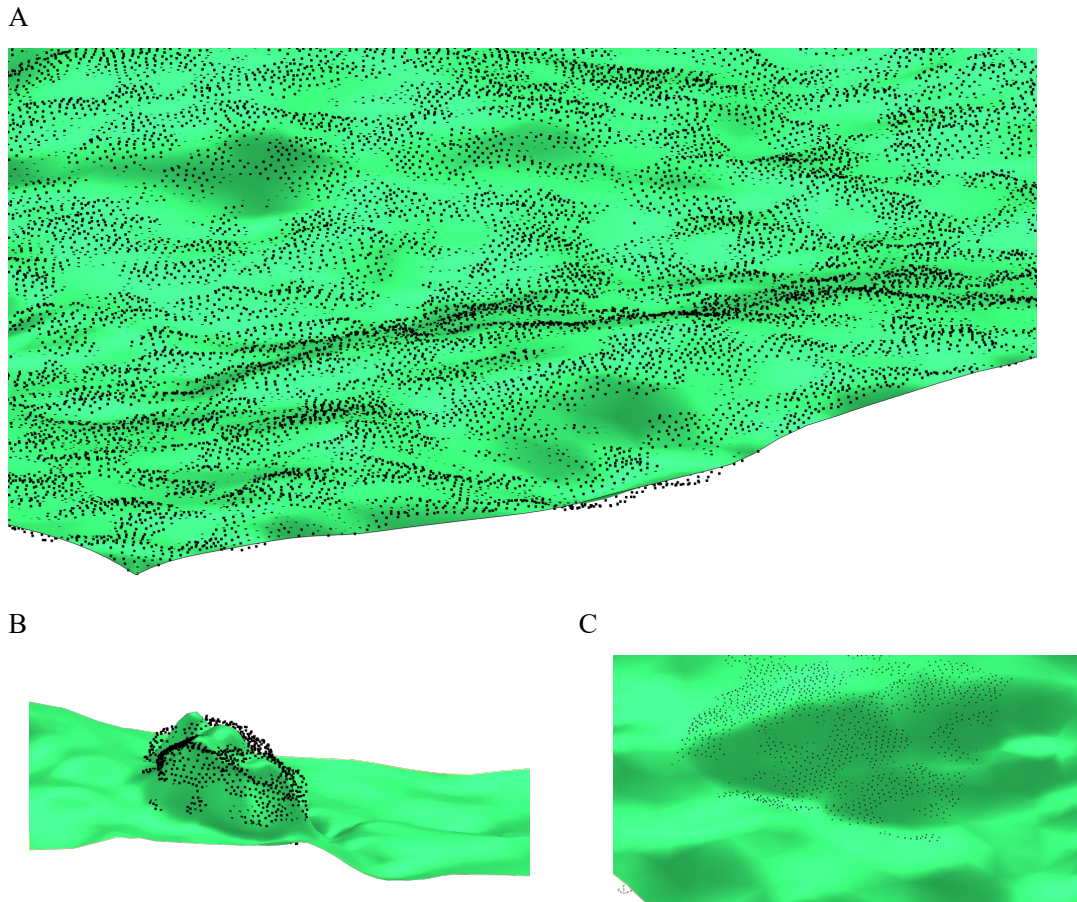


Figure 3-4. Visualisation of the original points (black) and the surface that we interpolated in COMSOL Multiphysics. A) an overview of a larger section of the geometry, B) a close-up of an area where the original data was very uneven, and C) an area where the original data was fairly smooth.

In the *Parallel Plate Model*, the location of the top surface was parametrised so that the deviations and rotations could be automated using MATLAB and the model then run in COMSOL Multiphysics subsequently. The parameters were varied based on the Design of Experiments (DoE) scheme Definite Screening Designs (DSD) presented in Section 3.1.6. As the sensitivity analysis varies the location of the top surface, it had to be ensured that the aperture dimensions, and more specifically the inlet and outlet areas, remained comparable. Thus, maximum aperture extents were calculated based on the x-, and y-deviations and rotations around the z-axis. An exaggerated demonstration of this is presented in Figure 3-5.

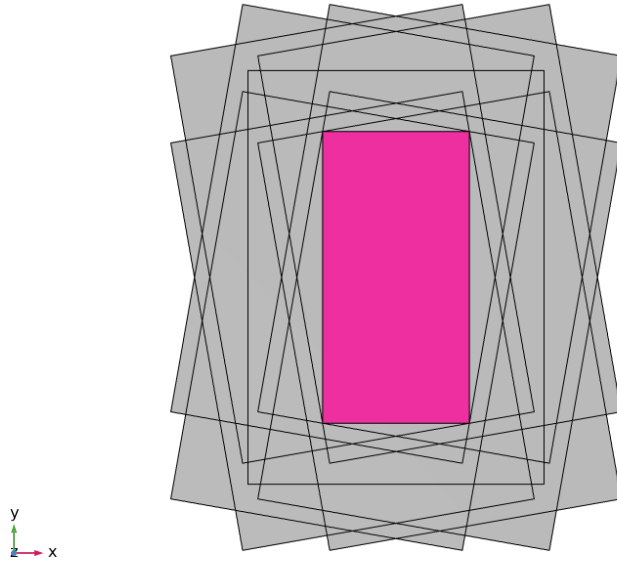


Figure 3-5. An exaggerated visualization on how the maximum common aperture was determined for the sensitivity analysis. The pink area corresponds to the maximum common aperture, when one of two surfaces is moved in x -, and y -, directions and rotated around the z -axis.

The void space between the bottom and top surfaces whose coordinates were based on the DoE was then converted into a 3D fracture geometry, which was filled with water. The mesh generation was also automated for all variations of the geometry, by creating a triangular mesh on the top and bottom surface and a free tetrahedral mesh in between them. The detailed modelling parameters, including the mesh details, are presented in Section 3.1.4.

As output variables for the *Small Surface Model*, the flow rate and a measure for flow channelling were calculated as follows:

$$F = \frac{1}{A} \int_A \frac{|v - v_{avg}|}{|v_{avg}|} dS, \quad (10)$$

where A is the area of the outlet of the flow channel, v the velocity at a point on the surface and v_{avg} the average velocity at the outlet. The flow channelling measure F differs from the channelling factor in Equation (18) that was later defined in the Task Description and the 3D adoption to it in this report, Equation (19).

Contact models:

The *Nearing* and *Departing Contact Models* were aimed to represent the experimental setup in detail. The models consist of two consecutive models. In the first one, contact between the upper and lower rock part is modelled. The deformation of the rock parts is calculated based on the contact. In the latter model, fluid flow is simulated in the deformed void space between the rock parts.

In order to create the contact model, a rock geometry had to be defined. The scanned fracture surfaces provided in the data delivery by the Task Description were imported to COMSOL Multiphysics. The surfaces were again converted into parametric surfaces (cubic spline interpolants of the measured data) as in the *Small Surface Model*. Initially, the parametric surfaces extended from 0 mm to 200 mm in both x - and y -directions. The resulting surface is visualized in Figure 3-6. As it can be seen, sharp peaks in z -direction are apparent at the surface edges. These were created as the sample is not precisely 200 mm wide or long, and thus the scanning data includes parts of the sides of the rock sample. To remove these deviations in z -direction, the sample was trimmed by 1 mm both in x - and y - directions.

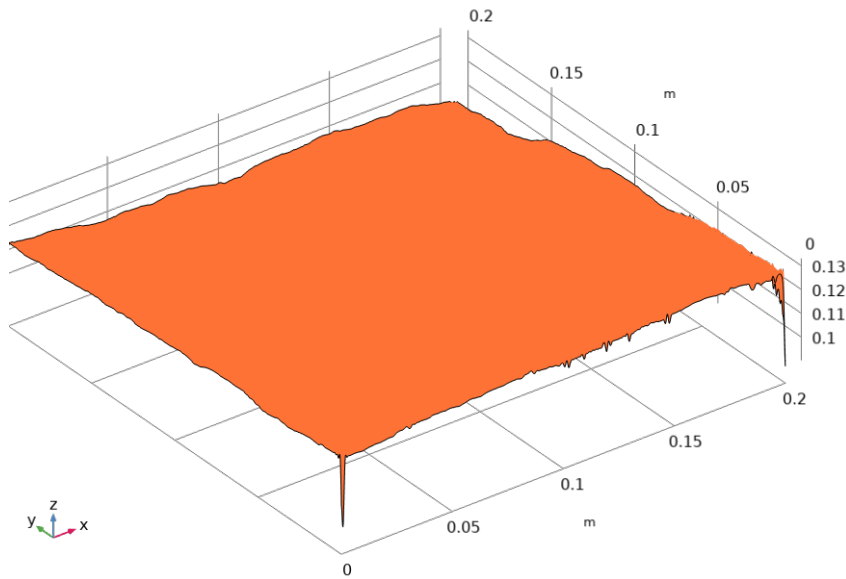


Figure 3-6. The created parametric surface of the bottom fracture surfaces. Large deviations in the z-direction are visible on the edges in areas where the sample is less than 200 mm wide.

When numerical representations of the surfaces were created and placed in their provided locations, some overlap between them was observed as seen in Figure 3-7. In the Kalmar Task Force meeting, it was discussed how some permanent deformation had presumably already occurred during splitting of the rock parts prior to scanning the surfaces. Not only was force needed to open the rock, also some parts were chipped off. During this process, it is likely that some rock parts deformed permanently but did not chip off meaning that this permanent deformation would have been included in the surface scan data. Consequently, the permanent deformation due to the opening of the fracture may have caused some overlap between the numerical representations of the top and bottom fracture surfaces when they were placed on their corresponding coordinates. It is possible that the permanently deformed (but not chipped off) rock could compress easier back to its original shape when the top and bottom domains were compressed together again. For example, if the permanent deformation was volume dilatation due to new microfractures opened by tensile stress, the microfractures could have been closed during the compression. It is also possible that the overlapping areas are the chipped rock pieces that were identified in the Task Description, if the surface scanning was performed before chipping. Surface scan accuracy could also partly explain the overlap. In any case, the overlapped areas seemed extra rock that should be removed. If no actions were not taken, there would be high stress concentrations located in the areas with the overlap, and the top and bottom rock parts in the model would farther away from each other than measured in the experiment. This would leave a larger than expected aperture distribution between the surfaces leading to higher flow rates.

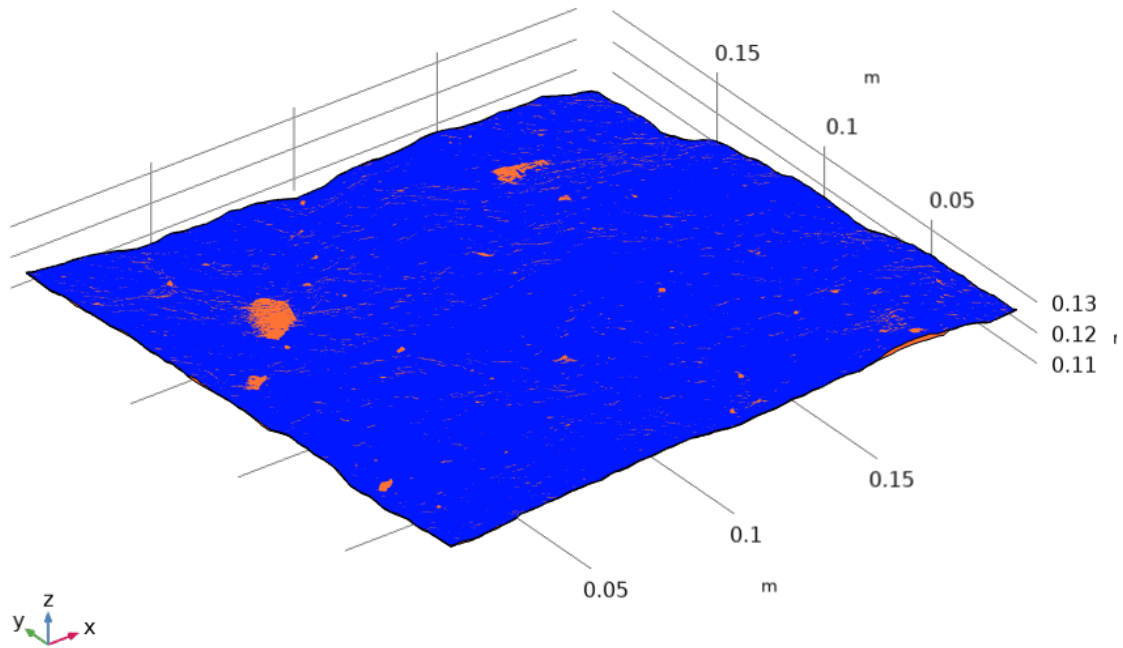


Figure 3-7. Both created parametric fracture surfaces are placed on their correct locations. The bottom surface (orange) is clipping through the top surface (blue) in some areas.

One solution could be considering the overlapping areas to be weaker during the contact modelling, but as no measured data for any mechanical parameters of the stiffness of the damaged areas was available, this approach was not used. Instead, the areas with the overlap were trimmed. The approach is visualised in Figure 3-8. All areas, where the bottom fracture surface (B) would clip over the top surface (A) were removed from B. Correspondingly, all areas of A clipping B were removed. In the removed areas the clipped surface would follow the other surface. Thus, the surfaces would be in contact when the surfaces are placed in their corresponding locations.

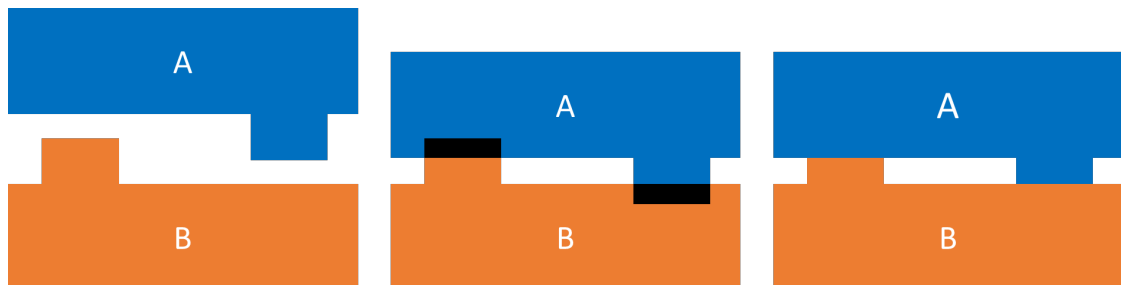


Figure 3-8. Illustration on how clipping of overlaps between the initial surfaces are handled. The blue part (A) corresponds to the top surface while the orange part (B) corresponds to the bottom surface. In the middle, the two surfaces are placed on their respective coordinates and their overlap is presented with the black colour. On the right, areas of A that were clipping into B and vice versa have been removed.

After the surfaces were created and trimmed, a 250 mm tall rock block was created. This block was then split into two parts using the two trimmed fracture surfaces. This resulted in the final model geometry as seen in Figure 3-9.

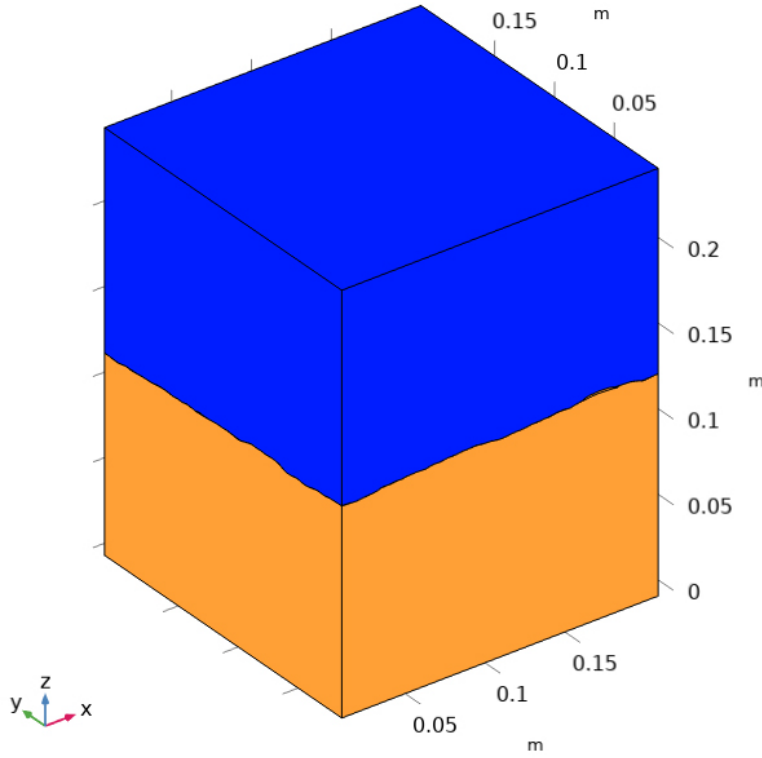


Figure 3-9. Final model geometry. The blue part corresponds to the top rock part in the experiment while the orange to the bottom rock part. The fracture surfaces are situated on the border between the blue and orange part.

In the contact models, the force balance equation (7) is solved. Additional boundary conditions were also required. First, a contact pair was defined between the bottom and top fracture surface. The contact formulation aims to prevent the upper rock part geometrical domain from entering the lower rock part domain. Instead, increased stress is induced in areas of contact in both the upper and lower rock parts. Consequently, the rock parts deform elastically. The contact formulation was calculated using the so-called augmented Lagrangian contact method (COMSOL, 2022a, Chaboche et al., 2001). In this method, the contact pressure (T_{np}) between the top and bottom domains is calculated using:

$$T_{np} = \begin{cases} T_n - p_n d_g, & \text{if } d_g \leq 0 \\ 0, & \text{otherwise} \end{cases}, \quad (11)$$

where T_n is an initial guess for the contact pressure (1 GPa), used for speeding up the convergence. The penalty factor (p_n) is a function of an equivalent Young's modulus of the material, E_{char} , and the minimum element size on the destination surface, h_{min} :

$$p_n = \frac{E_{char}}{h_{min}} \quad (12)$$

and d_g is the gap between the domains:

$$d_g = g - d_{offset}, \quad (13)$$

where g is the true gap between the domains and d_{offset} is an offset value that can be used, for example, to prevent overlap between the two domains (COMSOL, 2022a). The offset value is needed, as the contact formulation does not always prevent overlap of the two domains perfectly due to imperfect numerical representation of fracture surfaces and due to remaining numerical error. Used model parameters are presented in Section 3.1.4. The contact gap acts as a major limitation of the contact modelling, as it induces a larger aperture and consequently a larger flow rate in contact models.

Two different approaches in contact modelling were utilized. In the first approach (*Nearing Contact Model*), the two rock parts are initially separated by a small gap. The top rock part is then compressed with a constant normal load towards the bottom rock part, until the gap is closed, and the model reaches equilibrium. Due to the initial gap, no counterforce exists initially for the top part. This can cause the model to have problems finding an initial answer (rigid displacement is not constrained). Thus, a *spring foundation* function is applied to the top part. This causes the top part to act as a spring with a set spring constraint in the z direction (upwards and downwards). The spring is expressed simply as Hooke's law:

$$F = -kz, \quad (14)$$

where z is the displacement of the domain in z -direction and k the spring constant. This spring foundation is then gradually decreased to 0 in discrete steps so that the contact problem is solved with a nonlinear solver at each step (with constant spring constant at that step) and the displacement from the previous iteration is used as initial guess for the next. This causes the spring to become less stiff and the top domain to move closer towards the bottom domain, eventually leading to contact without the effect of the spring. The spring constant is changed with the following relationship (COMSOL, 2022b):

$$k = k_0 \cdot (1 - R) \cdot 2^{-10R}, \quad (15)$$

where k_0 is the initial spring constant, set to a high value and R a constant that is being increased from 0 to 1.

In the second contact approach (*Departing Contact Model*), the top part initially overlaps with the bottom part artificially without an applied spring foundation. The contact formulation then forces the top part to move upwards until an equilibrium with the normal load and the contact pressure is reached. The benefit of the second approach is that less iterations are needed to model the contact problem.

In addition to the contact formulation, other boundary conditions were also defined. On the bottom surface of the lower rock part, a fixed constraint is used ($\mathbf{u} = 0$). This prevents any movement of the surface in any direction. On all sides of both rock parts, a roller condition ($\mathbf{u} \cdot \mathbf{n} = 0$) is used. This allows movement of the surfaces only in z -direction. Finally, on the top surface of the upper rock part, a normal load was defined:

$$\boldsymbol{\sigma} \cdot \mathbf{n} = \mathbf{F}. \quad (16)$$

The geometry was discretized with a finite element mesh. In the *Nearing Contact Model*, the top fracture surface was meshed with a free triangular network with a minimum size of 0.5 mm and a maximum size of 1 mm. The bottom fracture surface was also meshed with a free triangular network. In order to gain a better convergence with the contact problem, it was suggested by COMSOL (2022a) that the mesh density would be doubled on the destination surface in the formulation. Thus, a minimum size of 0.25 mm and a maximum size of 0.5 mm were used. The remaining geometry was meshed with a free tetrahedral mesh. The finalised mesh is presented in Figure 3-10.

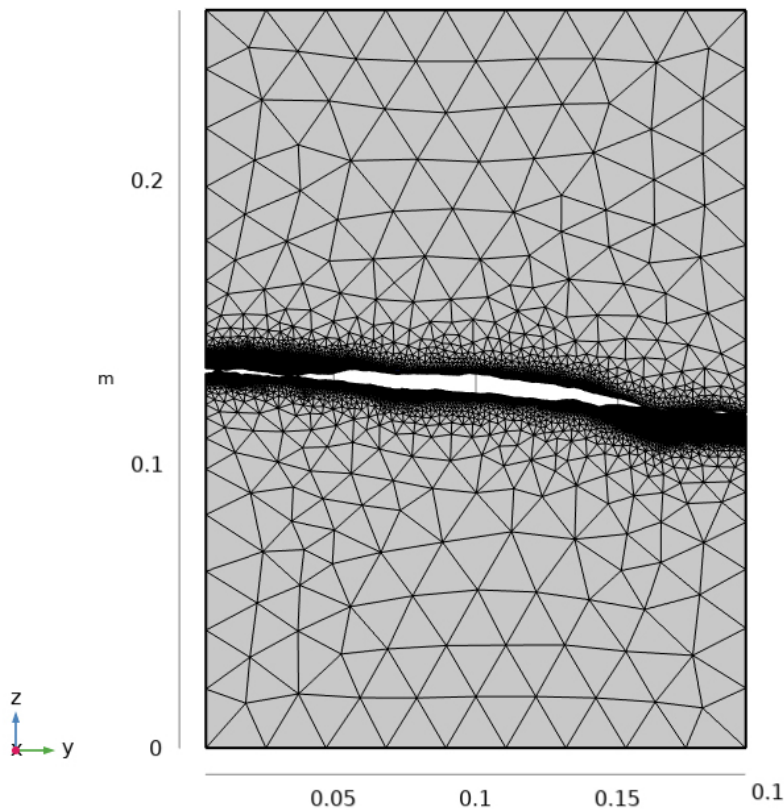


Figure 3-10. Finalised mesh from the side for the first contact model approach (*Nearing Contact Model*). Note that there is an initial gap between the bottom and top rock parts causing the large aperture.

Similarly, in the *Departing Contact Model*, a free triangular mesh was created for the fracture surfaces. For the model, the minimum element size was 0.1 mm and the maximum element size 1 mm for both surfaces. This mesh was used for 0.1 mm and 0.05 mm contact offset values (presented in Section 3.1.4) and runs with different normal loads. The rest of the geometry was meshed with a free tetrahedral mesh. The total element count of the mesh was 1,851,901.

For both contact models, an identical solver setup was used. The settings were the same as with the *Parallel Plate Model* described above.

Both contact modelling approaches were successful in creating a deformed void space geometry as discussed in Section 4.2.1. The resulting deformed geometry was re-meshed and utilized in creating the fluid flow model. In general, first the new mesh is imported into a separate geometry sequence. There the void space is turned into a geometric entity. After that, material properties and boundary conditions were again defined and finally a new mesh created.

The deformed geometry from both contact model approaches was re-meshed with a triangular network on the fracture surfaces and a free tetrahedral mesh elsewhere. The triangular mesh on the upper fracture surface in the *Nearing contact model* had a minimum element size of 0.5 mm and a maximum element size of 1 mm. On the bottom surface the same properties were 0.25 mm and 0.5 mm. With the *Departing contact model*, the minimum element size was 0.05 mm and the maximum 0.5 mm with the 0.1 mm contact offset and 0.03 mm and 0.3 mm with the 0.05 mm contact offset on both surfaces. The free triangular meshes were then refined for the *Departing Contact Model* by splitting the longest side of each element into two. The number of elements in the mesh was 5,448,370 for the *Nearing Contact Model*, 3,538,629 for the 0.1 mm contact offset, and 11,380,203 for 0.05 mm contact offset using the *Departing contact model*. The difference in mesh density was a result of the contact gap distance being smaller in the second contact approach (0.035 mm versus 0.1 mm) and the model was prone to geometric overlap otherwise.

The meshes of the deformed geometry were turned into a 3D-geometry consisting of solely the void space. The geometry at the inlet was extruded by 30 mm in order to allow for a fully developed flow to enter the actual void space. Material properties of water (Section 3.1.4) were assigned to the model. As with the *Parallel Plate Model* discussed above, Equation (6) is solved and Equation (9) used as a boundary condition on the walls of the geometry. Again, the average values of inlet and outlet pressures were used (Section 3.1.4).

For both models, the void space geometry was meshed by first assigning a free triangular network on both the bottom and top surface of the geometry. A minimum element size of 0.1 mm and a maximum element size of 0.5 mm was used for the *Nearing Contact Model* and 0.05 mm and 0.5 mm, respectively, for the *Departing Contact Model*. For the latter, also a mesh refinement tool was used. It splits the longest side of the triangles into two creating two elements out of one. This refinement was used to prevent meshing overlap in the finalised geometry. In subsequent models, where the normal load was increased, the element size on the bottom surface was further decreased to 0.25 mm and 0.025 mm. The domain between the fracture surfaces was then meshed with a free tetrahedral mesh. Additionally, two thin boundary layers were assigned near the fracture surfaces to better account for slower flow near the walls due to parabolic flow profile in the *Nearing Contact Model*. In the *Departing Contact Model*, these were not added as the aim was to reach a smaller contact offset with a lower number of elements. The total mesh element counts were 2,450,718 and 3,536,631 for the different methods when using a 0.1 mm contact offset. The mesh density varied slightly when different normal loads or contact offsets in the *Departing Contact Model* were used. With 0.25 mm minimum element size on the bottom surface, the mesh element count was 10,357,408. The finalised mesh of the *Nearing Contact Model* is presented in Figure 3-11.

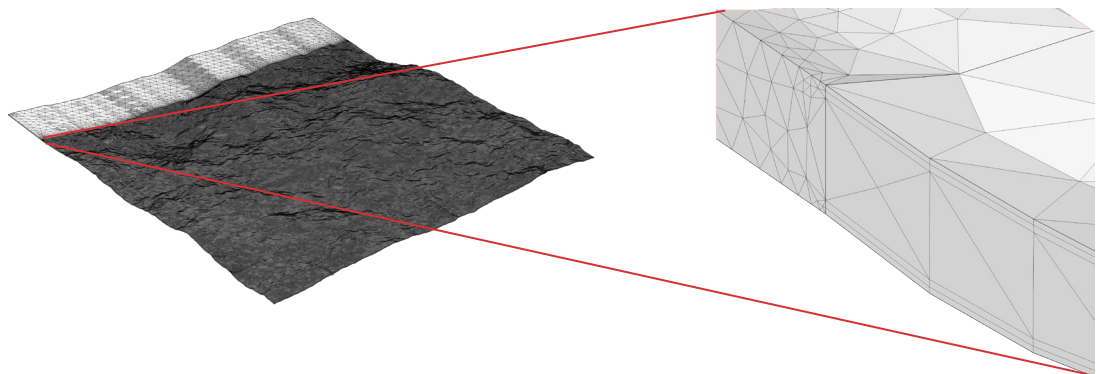


Figure 3-11. Finalised mesh of the fluid flow geometry based on the *Nearing Contact Modelling* approach. On the left the full extent of the mesh and on the right mesh where the extruded inlet and the fracture void space geometry meet.

3.1.3 Determination of critical aspects

Critical aspects of the modelling approach mainly relate to the unknown aspects and scanning of the fracture surfaces. The surface geometry depends both on the scanning precision and -resolution. Thus, the geometrical data is only a representation of the real fracture geometry.

Some rock deformation occurred during opening of the fractures. This also leads to uncertainties in the fracture surfaces if they are used as a geometry for a model of an unopened case. Furthermore, the opening of the rock caused permanent deformation of the rock which might lead to smaller simulated apertures when the rock sample is compressed virtually in a contact model. Some permanent deformation could also occur during the compression itself.

Another critical aspect is the placement of the fracture surfaces on top of each other during modelling. The surfaces were placed based on the coordinate data of the surfaces. If this data does not fully represent the actual placement of the surfaces during the experiment, it could have an effect on the resulting flow rates.

Assumptions of the fracture were also made. These included that the fracture is devoid of any filling minerals. However, the possibility of such minerals was presented in the Task Description.

3.1.4 Model parameters

In this section, the parameters used in the five different models are presented.

Analytical Model:

$$Q = W \cdot \frac{d^3}{12\mu} \left| \frac{\partial p}{\partial x} \right| \quad (17)$$

As seen in Equation (5), an aperture, channel length, pressure difference between the inlet and outlet, and a fluid viscosity are required for determining a flow rate. The aperture was varied between 0.001 mm and 0.01 mm as discussed above. The flow channel length was selected based on the rock sample length of 0.2 m from the Task Description. The pressure difference was calculated based on the average inlet pressure of 0.3882 bar (38.82 kPa) and outlet pressure of 0.0699 bar resulting in $\Delta p = 0.3183$ bar. Lennon (2014) presents a dynamic viscosity of water of 1.0016 mPa·s at 20°C. This value was used for the *Analytical Model*.

Parallel Plate Model:

In the first numerical model, the *Parallel Plate Model*, the model consists solely of water. The water is assumed to be 20°C with a density of 998.20 kg/m³ and a dynamic viscosity of 1.0093 mPa·s. The density and dynamic viscosity were selected based on the COMSOL (2022a) default values. From the data provided by the Task Description, again the average inlet and outlet pressures were used being 0.3882 bar at the inlet and 0.0699 bar at the outlet.

Small Surface Model:

The objective of the *Small Surface Model* was to perform a sensitivity analysis on the placement of the top fracture surface on the bottom surface. The fracture void space geometry was varied based on deviations of the top surface placement in *x*-, *y*-, (horizontal directions) and *z*- directions and rotations around the *z*-axis.

0.05 mm deviation in the horizontal directions, 0.01 mm in the *z*-direction, and 0.5° rotation were selected for the sensitivity analysis. These values were varied by multiplying them with -1, 0 or 1 according to the selected three level Definite Screening Design (Jones and Nachtsheim, 2011 and 2013). The resulting parameter combinations are shown in Table 3-1.

Table 3-1. The parameter combinations according the Definite Screening Designs.

Run	$\Delta x(\text{mm})$	$\Delta y(\text{mm})$	$\Delta z(\text{mm})$	$\Delta \text{rot}(\text{°})$
1	0	0.05	0.01	0.5
2	0	-0.05	-0.01	-0.5
3	0.05	0	0.01	-0.5
4	-0.05	0	-0.01	0.5
5	0.05	0.05	0	0.5
6	-0.05	-0.05	0	-0.5
7	0.05	-0.05	0.01	0
8	-0.05	0.05	-0.01	0
9	0.05	-0.05	-0.01	0.5
10	-0.05	0.05	0.01	-0.5
11	0.05	0.05	-0.01	-0.5
12	-0.05	-0.05	0.01	0.5
13	0	0	0	0

The maximum fracture dimensions were also calculated based on the maximum and minimum deviations. The resulting fracture was 69.036 mm wide and 99.300 mm long. The upper surface was moved upwards by the thickness of the spacer ring (9.92 mm) to properly reference the data as discussed in the Task Description. Material properties of water were again assigned to the domain and based on COMSOL Multiphysics default values at 20°C (see *Analytical Model* parameters).

Finally, the meshing sequence was automated so that it would be created based on identical starting parameters for each run. A free triangular network was defined on the fracture surfaces with a minimum element size of 0.05 mm and a maximum element size of 0.5 mm. The volume between the surfaces was meshed with a free tetrahedral mesh. The total element count, however, depended on the parameters of the sensitivity analysis run.

Contact models:

In both the *Nearing contact* and *Departing Contact Models*, the upper and lower parts consist of homogenous rock. The Task Description provided the rock mechanical properties. These include the uniaxial compressive strength (UCS), Young’s modulus and Poisson’s ratio. As the rock is assumed to be linear elastic in this study, the UCS was not utilized in the mechanical modelling. Used average values that were determined normal to the fracture surfaces are presented in Table 3-2. The uniaxial compressive strength is only used in result analysis. In addition, a density of 2,600 kg/m³ (Geological Survey of Finland, 1997) for the rock was used.

Table 3-2: Rock mechanical parameters used in the numerical model.

Parameter	Value	Unit
Young’s modulus	72.9	GPa
Poisson’s ratio	0.31	-
Density	2600	kg/m ³
Uniaxial compressive strength	271	MPa

Fluid properties were also shared between both approaches. The temperature was again assumed to be 20°C and the resulting density and viscosity 998.20 kg/m³ and 0.0010093 Pa·s.

Nearing Contact Model:

In addition to the shared model parameters, the *Nearing Contact Model* had parameters for the spring constant in Equation (15). In the equation, the spring constant used in the spring foundation is iteratively decreased so that R increases from 0 to 1. As the initial spring constant per unit volume k_0 , a value of $1E12 \text{ N/m}^4$ was used.

Additionally in Equation (13), a contact offset was defined. This offset is used to force two parts, in this case the bottom and top rock part, to have a minimum gap between their geometries when compressed together. If such offset would not be used, it would be possible that the geometries would overlap partially after the contact model has been calculated. The overlap does not prevent the contact problem from converging, but as the finished geometry of the contact model is used as the basis for fluid flow modelling in the deformed geometry, the overlap has to be prevented. In the *Nearing Contact Model*, a contact offset (d_{offset}) of 0.1 mm was used. A large value was selected due to preliminary tests showing issues in convergence in the contact model using small contact offset values. The large contact offset was the main driver for an updated contact formulation, the *Departing Contact Model*.

Departing Contact Model:

Similarly to the *Nearing contact model*, a contact offset was defined in the *Departing contact model*. As the calculation times were much shorter on the latter, a smaller offset value that would still not have any geometric overlap, was sought. The target offset value was 0.035 mm which would correspond to the measurement precision defined in the Task Description. This value was used instead of zero, since early model testing showed that too small contact offset may lead to convergence issues in the contact model as well as to problems when creating the flow model geometry and the added error is less than the error due to the measurement precision. In the end, the smallest contact offset value that was achieved was 0.05 mm. In addition, the model was run with 0.1 mm contact offset to have comparable results with the *Nearing Contact Model*.

The *Departing Contact Model* was also used to study how different normal loads affect the flowrates. Normal loads of 0.02 MPa, 2 MPa, 4 MPa, 6 MPa and 8 MPa were simulated using a contact offset value of 0.1 mm. The first normal load corresponds to the unloaded case where the upper rock part is put on top of the lower one without any applied load.

3.1.5 Identification of influential factors

The scanned point clouds representing the fracture surfaces are only estimations of the true fracture surface geometry with a specific precision and resolution. In our modelling approach, the fracture surface scans were turned into parametric surfaces during importing. As discussed above, this had a smoothing effect on the fracture surface which, in turn, has an effect on the fracture aperture.

The effect of the experimental measurement precision was studied both with the *Analytical* and the *Small Surface Models*. With sufficient computational power it would be possible to use the original experimental data set for the fracture surfaces directly. It would be interesting to understand how large the effect of the surface parametrisation has in comparison to the experimental measurement precision, but the initial plan to study the effect with sensitivity analysis was not realised in the modelling process.

In our models, all rock deformations are considered elastic. This, however, does not necessarily represent how the rock deforms in the experiment. With the applied normal stresses, an assumption of linear elasticity can neglect the effect of the rock breaking at the contact points, possibly preventing the domains from compressing against each other as in the experiment. For a more accurate representation, the permanent deformation of the rock could be modelled. However, this is computationally demanding and, combined with the contact modelling itself, was not possible within this study. Nevertheless, the stress distribution resulting from the contact modelling could be compared with the uniaxial compressive strength of the rock which was provided to the modelling teams. This way, it would be possible to estimate areas where permanent deformation could occur. In addition, the provided linear variable differential transformer (LVDT) data could be compared with the simulated deformation to gain a better understanding of how the rock mechanical model performs.

Furthermore, it is possible that some geometric overlap occurs during the contact modelling, despite the contact formulation acting against it. The overlap does not prevent the contact simulations from finding a solution, from which a stress distribution and a deformed geometry can be calculated. However, when the deformed geometry mesh is converted to a new geometry of the fracture void space for the water flow model, the geometry can have small overlapping areas, preventing a new mesh creation for the fluid flow problem. Large overlaps are detected by the software, and they can be eliminated, but if the overlaps are very small and thin, it becomes increasingly difficult to do so due to limits in geometric tolerances or mesh density or how the model geometry is transformed to a finite element mesh. The geometrical overlap is discussed in more detail in Section 5.

Some uncertainty may also arise from the material and modelling parameters. For water and rock, average values were used. Similarly, many assumptions regarding the nature of the fluid flow were made. Realistically, the fluid within the void space would also resist the load somewhat, but in our approach the effect was omitted. The water pressure could have an effect especially in the zero-load case (0.02 MPa normal load). The usage of average values and the assumptions was justified by the purpose of first creating a workflow for contact modelling. If a smoothly working model would be achieved, the variations in model parameters could be also analysed by a sensitivity analysis. However, due to the long computational times of the models, this was deemed unpractical for now.

Finally, the mesh density used in all numerical models can have an effect on the output values, such as the flow rate. In an ideal case, the mesh density would be increased until the output values change less than a value such as 1% between subsequent mesh densities. In practice, this was not possible due to denser meshes not being able to be used in a reasonable computational time. This adds to the uncertainty of the results.

3.1.6 Uncertainty analyses

The *Small Surface Model* in this study was created to address the uncertainties related to the placement of the fracture surfaces with respect to each other and the fracture surface scan precision and resolution. The used surface scan precision and resolution were the ones obtained with the smaller surface scans of Task 10.2.1 described in the Task Description. The scanning precision in that task was 0.1 mm. The general idea of the model was to vary input parameters of the upper surface location on the order of the measurement precision and resolution to see how they change the output variables. In this case, the output variable was a measure for flow channelling according to Equation (10). A regression model was then fitted to the data and the properties of the fit analysed with statistical methods.

A full sensitivity analysis would require running all the input parameter combinations, which might lead to a high number of simulation cases. For example, with four input parameters and three levels of values, the total number of combinations would be $3^4 = 81$. There are, however, ways to reduce the number of needed runs such that the effect of each input parameter on the output variable can be estimated independently. One such method is Definitive Screening Design (DSD; Jones and Nachtsheim 2011, 2013). The design allows the estimation of main and second-order effects and a complete de-aliasing of main and second-order effects of continuous parameters. It also allows for aliasing between second-order effects. The DSD used here was created with the Minitab (2021) software and resulted in the factors for x -, y -, z -, and rotational values (Table 3-1).

3.1.7 Workflow describing the modelling process

Our modelling team decided to approach Task 10.2.2c by simulating the deformation of the rock parts during compression and estimate the fluid flow in the deformed void space with a "physically as-accurate-as-possible" model approach, meaning that the basic physical principles behind the processes are followed (3D fluid flow, fracture surface contact modelling and rock deformation models) and reasonably accurate presentation of the real fracture surfaces are used. Such a methodology could not only predict flow rates under different normal loads but could also address the effect of geometry on flow channelling. The original aim was also to perform an extensive sensitivity analysis (with a final model) that would cover many of the uncertain parameters and modelling choices we made.

From the beginning, it was clear that we would not be able to use the exact fracture scan data in the modelling since the contact model simulations (especially with complicated rock mechanical models) would become heavy and time consuming to solve as well as possibly non-convergent. Moreover, the needed level of accuracy in presenting the fracture surfaces was not clear (whether the full scan precision and resolution were needed in the modelling) and was something to be studied. Consequently, the virtual fracture surfaces in the model should be interpolations of or fits to the original scan data. The chosen first approach was to use piecewise cubic spline interpolations that were considered as the most straightforward option with our chosen simulation software after some other attempts (for example, using CAD software and Matlab to create the virtual fracture surfaces). The plan was to address uncertainties related to the interpolation with the extensive sensitivity analysis later. Similarly, the plan was to study the uncertainties due to mesh density in the same sensitivity analysis.

During the first attempts to create model geometries with the scanned fracture surfaces, the exact placement of the fracture surfaces on top of each other became an issue to solve. This was also discussed in the Task Force meeting #40 especially from the experimental uncertainty viewpoint. Consequently, our modelling team decided to run a preliminary sensitivity analysis concerning the surface placement. The sensitivity analysis model included only flow of water between the fracture surfaces, which were placed on top of each other such that there would be no overlap or contact between the top and bottom fracture surfaces. The setup was a natural starting point for the contact modelling, in which the aim was to follow the real process of placing the surfaces to contact with each other. Without any contact, the procedure, however, lead to a fracture void space that is likely too open. Consequently, the flow rates in the model would be higher than in reality.

Another aim of the sensitivity analysis was to set up the needed tools and automated computing processes for the further extensive sensitivity analysis (which were never realised due to the convergence problems with the contact models and limited resources). Resulting from the aim, the subsequent models inherited the way the fracture surfaces were treated as single geometric objects in COMSOL Multiphysics instead of, for example, splitting the surfaces to smaller areas when importing the surface scan data. Similarly, manual fine tuning of the model geometry or manual definitions of model parameters for specific areas in the model (for example, in the contact gaps) was tried to be avoided to allow for automation of the modelling with different model parameters. This would ensure that issues such as problematic areas of the mesh would be treated always with the same methodology without human subjectivity. Such treatment could be for example making the mesh denser locally close to the problematic areas.

The trial contact modelling was performed using the small fracture surfaces (from Task 10.2.1). With them, the developed *Nearing Contact Modelling* approach worked fine, and the computational times were reasonable. Thus, the same approach was used for the larger fracture surfaces (in Task 10.2.2). Enlarging the fracture surface size and having possibly more complicated fracture surfaces lead to increased computing times and frequent convergence problems with the contact modelling. This, in turn, lead to slow progress (in calendar time) in the model development since each model run took multiple weeks.

Another problem with the contact modelling was the need to use contact offset to be able to avoid geometrical overlap of the fracture surfaces in the subsequent water flow modelling. With realistically small offsets (on the order of the surface scan precision), the needed mesh density was impractical. Further, using the experimentally determined distance between the lower and upper fracture surfaces made the fracture surfaces overlap when they were virtually placed on top of each other (without normal loading). This suggested the rock pieces close to the fracture surfaces undergo permanent deformation when the rock halves are separated from each other. From several ideas and attempts to deal with the overlapped areas (e.g. considering using soft rock domains in the model and cutting the overlapped pieces out in different ways from the model geometry), the final outcome was the clipping method described in Section 3.1.2. Even with this approach, the fracture aperture likely remains too high if compared to experiment, due to too large contact areas preventing realistic compression of the rock. These two factors likely led to too large aperture void space and, consequently, too high flow rates when the simulations were compared to experiment (Section 4.2.1 and Section 4.3). The continuing convergence issues and long computational times with the *Nearing Contact Model* led to the development of the second contact modelling approach, the *Departing Contact Model*.

It was evident from preliminary tests with a simplified model geometry that overlap between two domains that are compressed against each other occurred if no contact offset was used. However, any added contact offset would also increase the resulting flow rate. As a compromise, the modelling team decided to start from a larger contact offset value to ensure that the model converges to a solution and then aimed for a lower value with consecutive model updates. During each model update, the contact model iterated from the initial rock domain position (domain apart from each other in the *Nearing Contact Model* and overlapping in the *Departing Contact Model*) towards the contact offset value. The target for the contact offset was set as the measurement precision of 0.035 mm. Ideally, an even lower contact offset value should be sought for so that its effect would be negligible when compared to the surface measurement precision, however lower numbers lead to overlap in the contact model preventing the creation of the fluid flow geometry.

With each model update of the contact model, the normal load on the top rock part was kept at the same value of 1 MPa. With the *Nearing Contact Model*, the contact offset used in the analysis was 0.1 mm. Due to the long computational time, no other offset distances were used and instead the *Departing Contact Model* was created. With that model, the contact offset was decreased from 0.1 mm towards 0.035 mm with consecutive model updates. The mesh was adjusted and made denser in between the model updates if needed for model convergence. The final contact offset value that was achieved was, however, 0.05 mm.

The first discussions on the flow rates in the fracture flow experiments (before the measurement results were revealed) suggested that our modelling results with the contact models were off by orders of magnitudes. The flow rates were measured in drops whereas the modelling results were significantly higher. Consequently, simple models for water flow between parallel plates (*Analytical Model* and *Parallel Plate Model*) were created to calculate what the assumptions and uncertainties in the performed modelling meant in terms of flow rates and in comparison to the measured values. With the *Analytical Model*, it was possible to estimate flow rates in smooth fractures with certain apertures. To analyse the effect of fracture surface scan precision uncertainty on the flow rate, the flow rate was calculated in a smooth fracture with effective aperture corresponding to the fracture surface scan precision. In principle, a zero (pointwise) aperture between the upper and lower fracture surfaces in the model could still mean an aperture of the measurement precision in reality (if the distance between two points is less than the measurement precision, they can be either on top of each other, the distance can be the measurement precision, or something in between). Therefore, this flow rate would give an estimate for the minimum error of the flow rate that is made in the modelling, if the fracture scan data is used.

Furthermore, a similar setup was created in the numerical modelling software to compare the analytical results of the flow between parallel plates to a similar setup in the software. With both the *Analytical* and *Parallel Plate Models*, the apertures presented in Table 3-3 were calculated. For both models, the outputs were flow rates corresponding to different apertures. Later, after the flow rate results of the POST experiment were published (results in Section 4.5 and discussion in Section 5), the *Analytical Model* was used to back calculate effective apertures that would result in similar flow rates. After the flow data reveal, the modelling was continued with the *Departing Contact Model* to understand why the predictions of flowrates were off by many orders of magnitudes. The model was run with 0.02 MPa (weight of the top rock), 2 MPa, 4 MPa, 6 MPa, and 8 MPa using a contact offset value of 0.1 mm, and the corresponding rock deformation was compared with the released LVDT data. Furthermore, the resulting stress states on the surfaces were compared with the pressure film results of described in the Task Description. A summary of all modelling steps is presented in Table 3-3.

Table 3-3: Modelling steps of this study.

Analytical Model
Calculation of flow rates with 0, 0.001, 0.005, 0.01, 0.02, 0.03, 0.035, 0.04, 0.05, 0.06, 0.07, 0.08, 0.09, 0.1 mm apertures
Back calculation by solving Equation 5 of equivalent parallel-plate apertures needed to reach flow rates of the POST Experiment under 1 MPa normal load
Parallel Plate Model
Numerical modelling of flow rates with 0, 0.001, 0.005, 0.01, 0.02, 0.03, 0.035, 0.04, 0.05, 0.06, 0.07, 0.08, 0.09, 0.1 mm apertures in a 200 mm x 200 mm void space
Small Surface Model
Defining a DoE (Table 3-1)
Numerical modelling of flow rates with x-, y-, and z-directional deviations and rotations around the z-axis based on the DoE
Analysing the flow rate results using Minitab
Nearing Contact Model
Numerical modelling of flow rates with fracture surface geometry based on the POST-experiment under 1 MPa normal load and 0.1 mm contact offset
Departing Contact Model
Numerical modelling of flow rates with fracture surface geometry based on the POST-experiment under 1 MPa normal load with 0.1 mm, 0.05 mm and 0.035 mm contact offset
Numerical modelling of flow rates with fracture surface geometry based on the POST-experiment under 0.02 MPa, 2 MPa, 4 MPa, 6 MPa and 8 MPa normal loads with 0.1 mm contact offset.

3.1.8 Pragmatic validation aspects

For pragmatic validation, the aimed validity rank for the contact models used for simulating the POST normal loading and flow experiment can be calculated as discussed in Section 2.4. The aim of our final model of Task 10.2.2c is to predict the flow rate and channelling of the flow in a mechanically coupled flow experiment ($m=3$). In the experiment, only the flow rate is measured (not the channelling) and, consequently, the model can only be validated with respect to flow. The initial zero normal load in the experiment allows validation of mechanically non-coupled flow model. The measurement of displacement in the experiment during normal loading allows validation of the mechanical model. Consequently, $n = 1$ (flow rate) + 1 (mechanical deformation) = 2. Increasing the normal load allows validation of the coupled model ($p = 1$ and the combinations of the phenomena altogether yields $m = 3$). As a consequence of these, the aimed validity rank is $2 \cdot 3^{(1+1)} = 18$.

4 Results

In this section, results for all models are presented. For each model, a flow rate is calculated for each aperture or normal load used in each case. The stress distributions from the contact models are also illustrated. In addition to the results of the numerical models, a channelling factor was calculated. The equation provided by the Task Description is based on Maillot et al. (2016):

$$d_{qnet} = \frac{1}{\sum S_m} \cdot \frac{(\sum S_m \cdot v_m)^2}{(\sum S_m \cdot v_m^2)} \quad (18)$$

where S_m is the area of a computing element and v_m the corresponding Darcy velocity of the element. The equation is intended for a 2D field and since our model is 3D, a 3D formulation was created:

$$d_{qnet, volume} = \frac{1}{\int_V 1 dV} \cdot \frac{(\int_V v dV)^2}{\int_V v^2 dV} \quad (19)$$

where v corresponds to the velocity of one computing element and $d_{qnet, volume}$ to the channelling factor in the entire volume. It should be noted that this formulation does not give a value of 1 even in a planar flow due to the parabolic flow profile.

4.1 Analytical Model

Results of the *Analytical Model* (cubic law) are presented in Table 4-1 and visualised in Figure 4-1.

Table 4-1: Calculated flow rates using the cubic law.

Aperture (mm)	Flow rate (ml/s)	Aperture (mm)	Flow rate (ml/s)
0	0	0.04	0.17
0.001	2.7E-06	0.05	0.33
0.005	3.3E-04	0.06	0.57
0.01	2.7E-03	0.07	0.91
0.02	0.021	0.08	1.36
0.03	0.072	0.09	1.93
0.035	0.11	0.1	2.65

Parallel Plate Model

The results of the *Parallel Plate Model* are visualised in Figure 4-1.

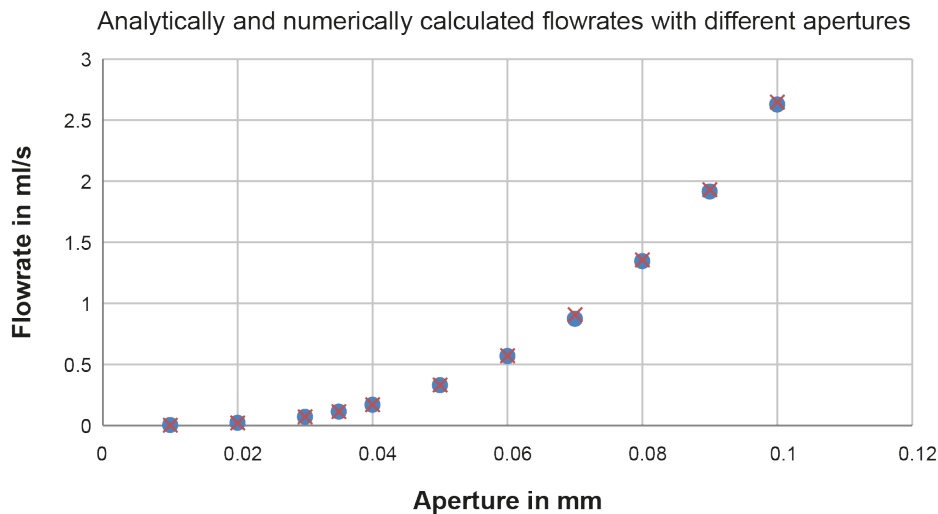


Figure 4-1. Comparison between the analytically and numerically calculated flow rates relating to different apertures in their corresponding void space. The dots correspond to numerical values and the crosses to analytical values.

Small Surface Model

The *Small Surface Model* was used to numerically calculate flow rates based on the x -, y -, and z -deviations and rotations around the z -axis as described in Table 3-1. The determined flow rates are presented in Table 4-2 and a streamline plot presented in Figure 4-2.

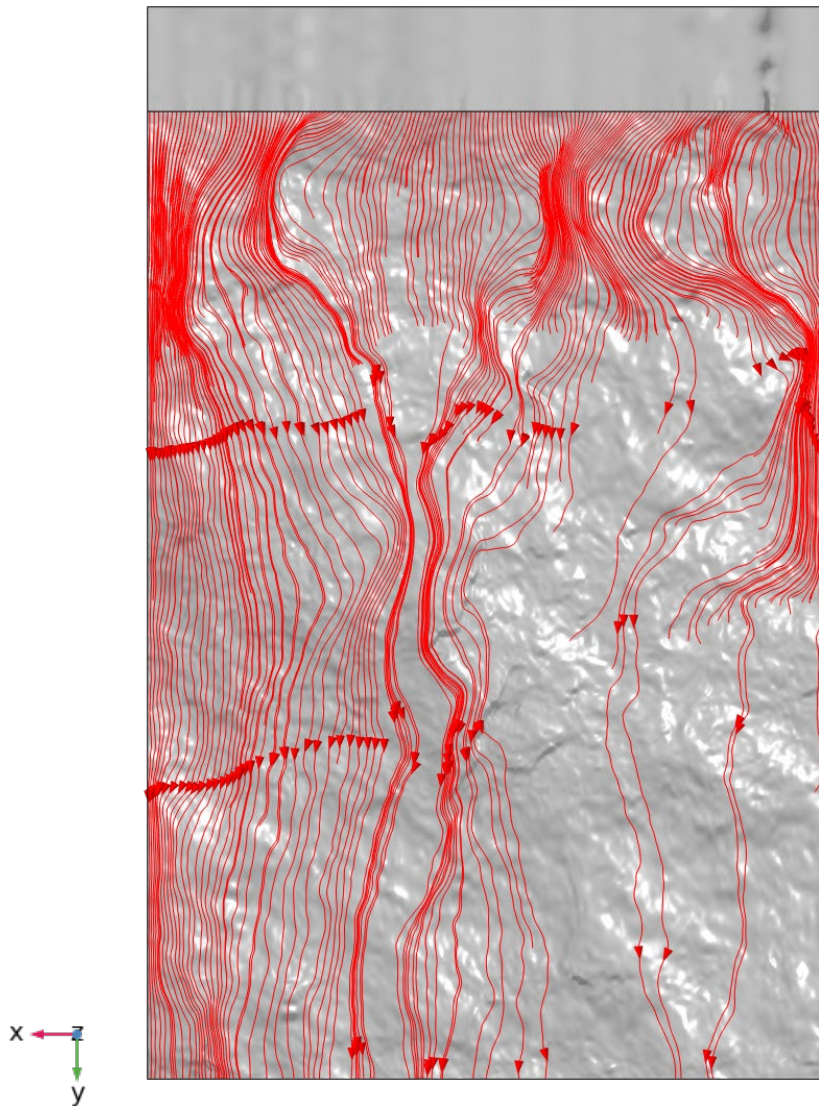


Figure 4-2. Streamline plot of the *Small Surface Model* with 0 mm Δx , Δy , Δz , and 0° Δrot on top of the modelled bottom fracture surface. The dead-end streamlines indicate areas where the streamline-pathing algorithm could not find a path forward.

Table 4-2: Results of the Small Surface Model where a sensitivity analysis was performed by varying x-, y-, and z- coordinates of the upper fracture surface and the rotation of the upper surface around the z-axis.

Run	$\Delta x(\text{mm})$	$\Delta y(\text{mm})$	$\Delta z(\text{mm})$	$\Delta \text{rot}(\text{°})$	Flow rate (ml/s)
1	0	0.05	0.01	0.5	0.5218
2	0	-0.05	-0.01	-0.5	0.5217
3	0.05	0	0.01	-0.5	0.5048
4	-0.05	0	-0.01	0.5	0.5443
5	0.05	0.05	0	0.5	0.5027
6	-0.05	-0.05	0	-0.5	0.5462
7	0.05	-0.05	0.01	0	0.5022
8	-0.05	0.05	-0.01	0	0.5421
9	0.05	-0.05	-0.01	0.5	0.5017
10	-0.05	0.05	0.01	-0.5	0.5422
11	0.05	0.05	-0.01	-0.5	0.5043
12	-0.05	-0.05	0.01	0.5	0.5461
13	0	0	0	0	0.5241

The results of the DSD were analysed with Minitab. A regression model in the form

$$y_i = \beta_0 + \sum_{j=1}^m \beta_j x_j^{(i)} + \sum_{j=1}^{m-1} \sum_{k=j+1}^m \beta_{j,k} x_j^{(i)} x_k^{(i)} + \sum_{j=1}^{m-c} \beta_{j,j} x_j^{(i)} x_j^{(i)} + \varepsilon_i \quad i = 1, \dots, n, \quad (20)$$

was fitted to the input parameter (Δx , Δy , Δz and Δrot) and output variable (flow rate) data (Table 4-3). The effects of each input parameter on the output variable represented using standardized effects, which are the regression coefficients corresponding to the input parameter divided with their standard errors (Figure 4-3). The significance of the regression fit in whole was tested with the F -test with significance level of $\alpha = 0.05$. It is tested if a trivial regression model (all coefficients are zero) would give a statistically significant fit to the data with significance level α . If not, a non-trivial fit would be more reasonable than the trivial one and the regression fit can be considered to have statistical significance.

Similarly, the significance of each input parameter in the regression fit is tested with the t -test with significance level $\alpha = 0.05$. It is tested if a trivial regression coefficient (zero coefficient) would give a statistically significant fit to the data with significance level α . If not, a non-zero regression coefficient would be more reasonable than zero coefficient and the regression parameter can be considered to have statistical significance. Corresponding to the t -test with $\alpha = 0.05$, a critical value for the standardized effects is shown in the pareto chart with a dashed vertical line. If the standardized effect is above this limit, it can be considered statistically significant.

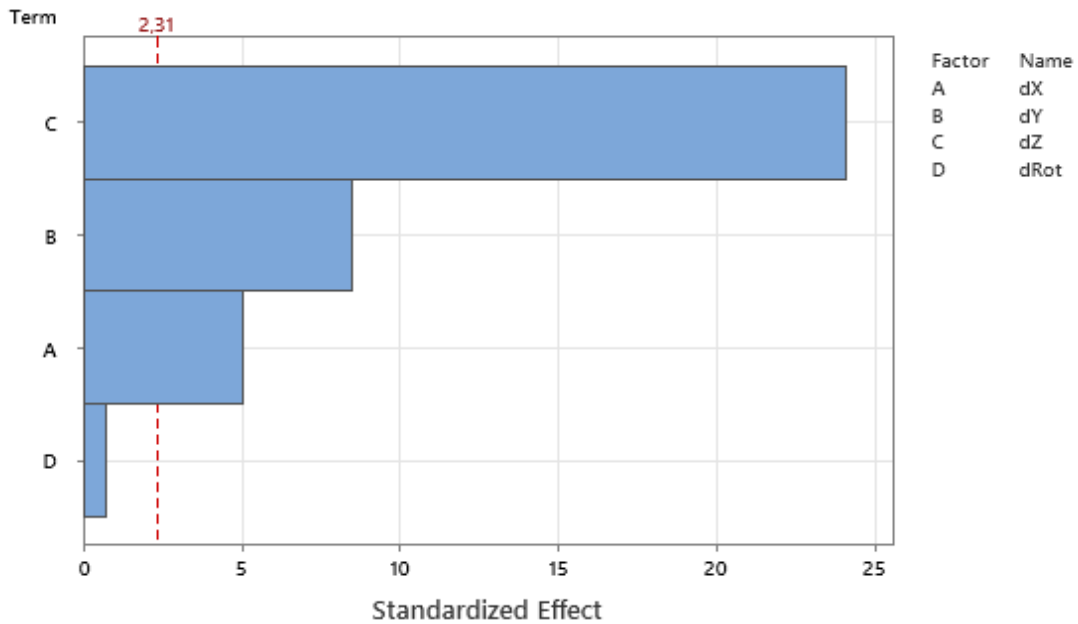


Figure 4-3. Pareto Chart of the Standardized Effects. The dashed line is the critical value for statistical significance according to the t-test with $\alpha = 0.05$.

The residuals (or errors) of the regression fit (difference between the fit and data) were analysed with the standard Minitab graphs (Figure 4.4) to see if the ordinary least squares (OLS) assumptions used in the fitting are followed. The Box-Cox transformed residual data (top left in Figure 4.4) shows that the residuals are approximately normally distributed (perfectly normally distributed residuals would follow the red line), which is one of the OLS assumptions.

With the residual versus fits graph (top right in Figure 4-4), it can be estimated if the residuals are randomly distributed and have constant variance (other OLS assumptions). The seen symmetry pattern indicates that higher-order terms could improve the fit, but with the small amount of data here, inclusion of more terms to the regression model could lead to overfitting. The histogram data (bottom left) is used to estimate if there are outliers or skewness in the residual data. However, with the small number of data points (less than 20), the histogram data does not reliably show these properties.

The residuals versus order plot (bottom right in Figure 4-4) is used to analyse if the assumption of the residuals being independent of each other is true. Ideally, the residual values would be randomly distributed around the centre value, but here the graph could be interpreted to have a trend, which would indicate correlation of the residuals of each other. Although not perfect, the residual analysis results were considered reasonable for the sensitivity analysis with the *Small Surface Model* at that point of the model development process.

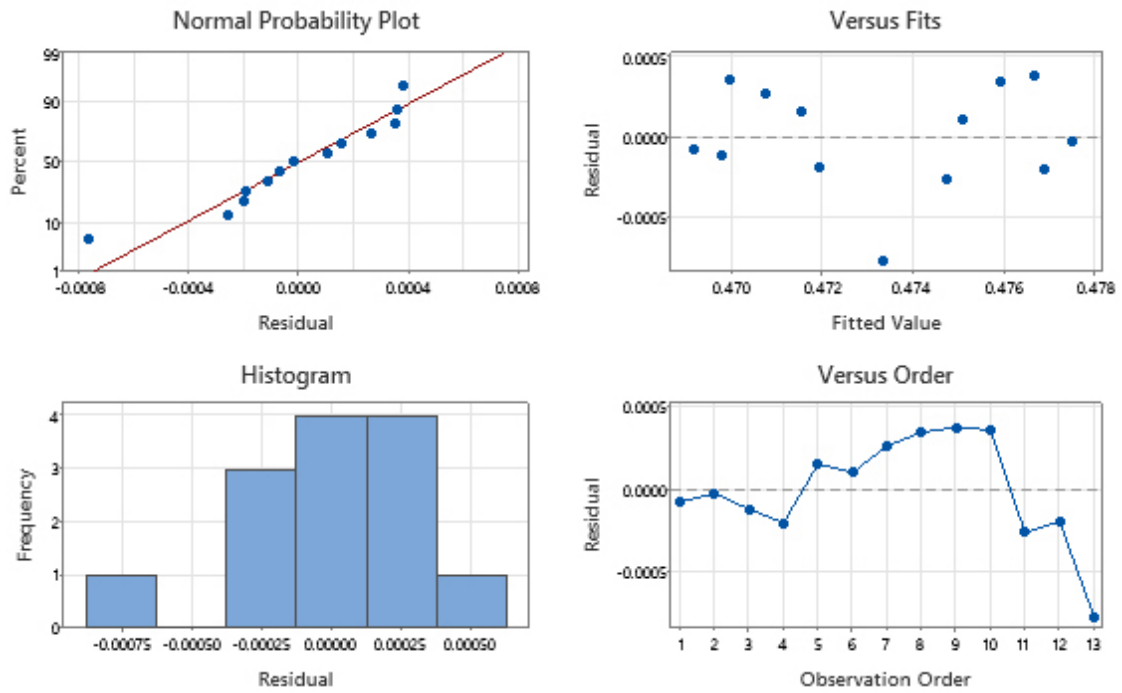


Figure 4-4. Residual plots of the DSD results. The residuals are the data pointwise errors of the regression fit, fitted values the regression fit constants, and the observation refers to the order of the regression fit constants.

4.2 Contact models

4.2.1 Nearing Contact Model

The *Nearing Contact Model* was able to find a solution to the contact problem with 1 MPa normal load. The calculation time for the contact model was approximately one month. The resulting stress state is presented in Figure 4-5. The contact offset distance used was 0.1 mm. Due to the long calculational time, successive runs with smaller distances were not calculated and instead the *Departing Contact Model* was developed.

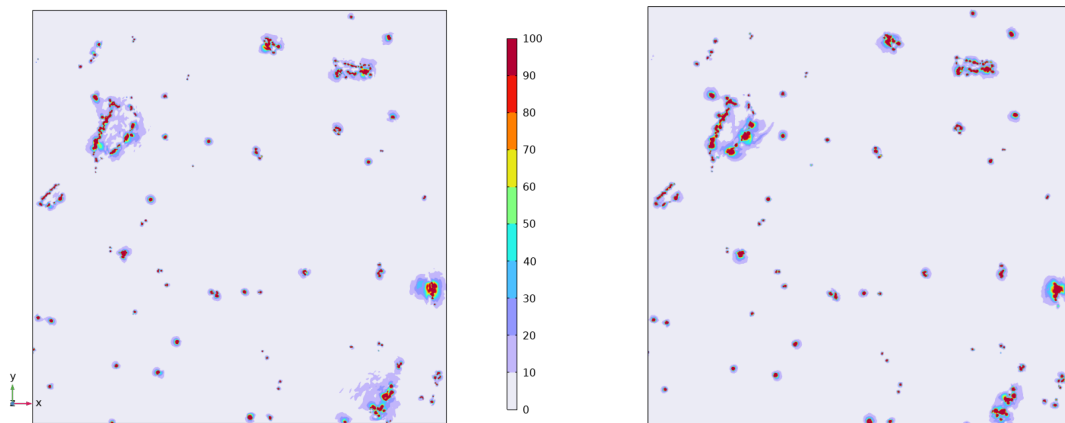


Figure 4-5. von Mises stress (MPa) on the fracture surfaces. The bottom surface is on the left and the top surface on the right. The different surface topologies result in slightly different stress accumulations. The scale was determined based on the scale used in the pressure film measurements in the Task Description.

Although no plastic deformation of the rock was modelled in our approach, the uniaxial compressive strength of the rock can be used to estimate whether permanent deformation would occur anywhere on the compressed rock sample. Thus, the stress distribution was again plotted in Figure 4-6 using the uniaxial compressive limit as the upper limit of the colour table range. The plot indicates that the rock would break at some of the contact points.

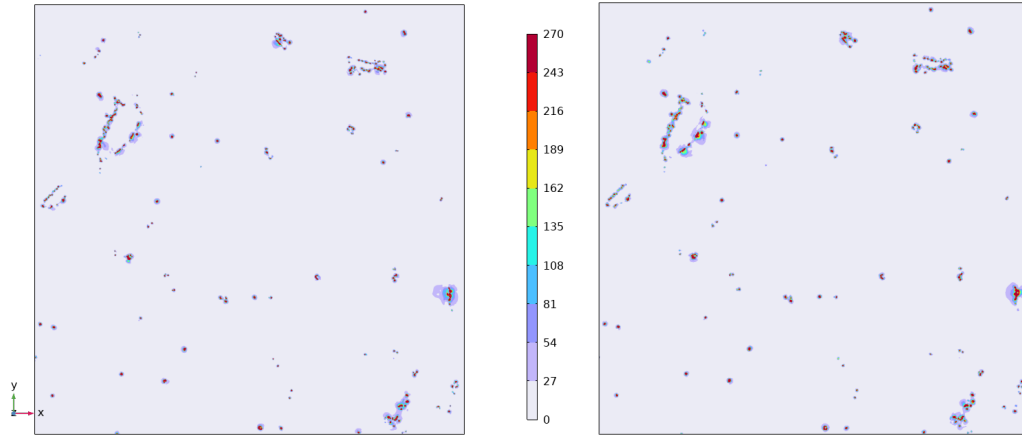


Figure 4-6. von Mises stress (MPa) on the fracture surfaces. The bottom surface is on the left and the top surface on the right. The different surface topologies result in slightly different stress accumulations. The scale was determined based on the UCS of the rock.

A deformed void space was created based on the contact model for which a visualisation with the created mesh was presented in Section 3.1.2.

The deformed geometry was used to simulate the water flow in 3D (see Section 3.1.2). To allow comparison to measured flow rates, the flow rate at the outlet boundary was integrated from the flow profile:

$$Q = \int_A v, \quad (21)$$

where v corresponds to flow velocity at a point at the outlet boundary, and A to the area of the outlet. The resulting flow rate was 137 ml/s. A visualisation of the flow in the void space is presented in Figure 4-7. The channelling factor was calculated using Equation (20) and was 0.64.

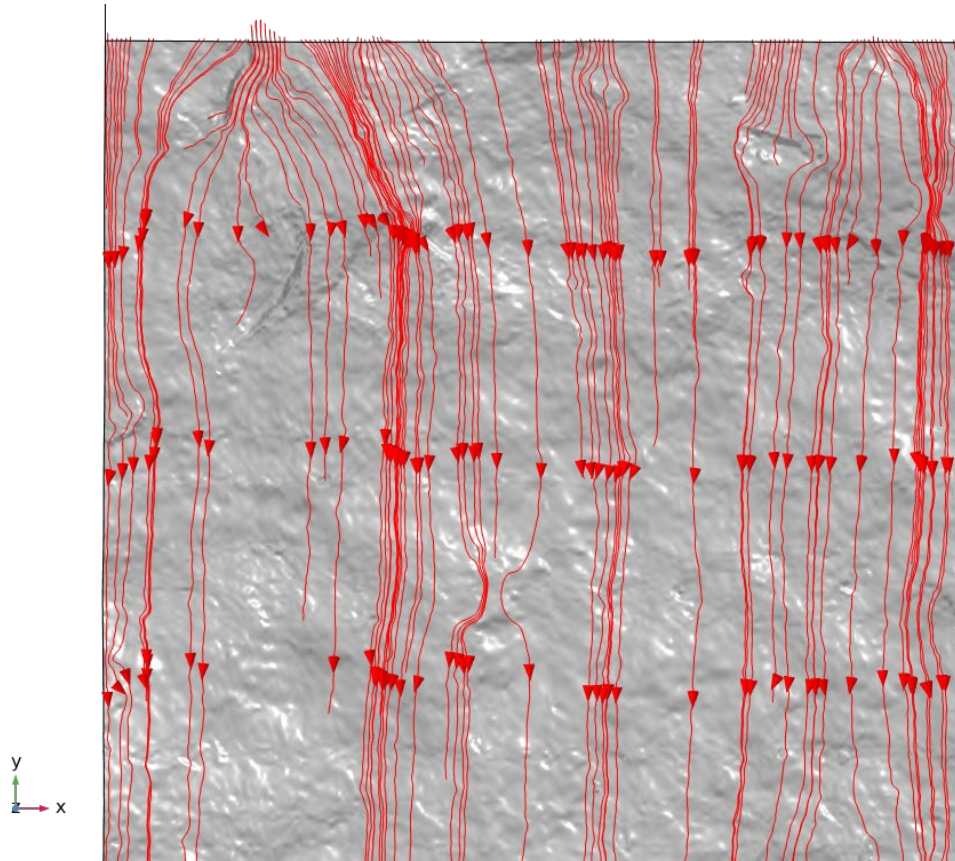


Figure 4-7. Streamline plot of the flow on top of the bottom fracture surface in direction from Face 2 to Face 4.

The aperture distribution on the outlet (from Face 3 to Face 1 in the Task Description) is plotted in Figure 4-8. The aperture was determined by performing a general extrusion from the bottom edge of the outlet so that it mapped the distance between the lower and upper edge of the void space. Based on the general extrusion, an average aperture of 0.050 mm was calculated. If this value is then inserted into the cubic law (Equation (5)) a flow rate between parallel plates with an identical effective aperture can be calculated. This flow rate is 0.33 ml/s.

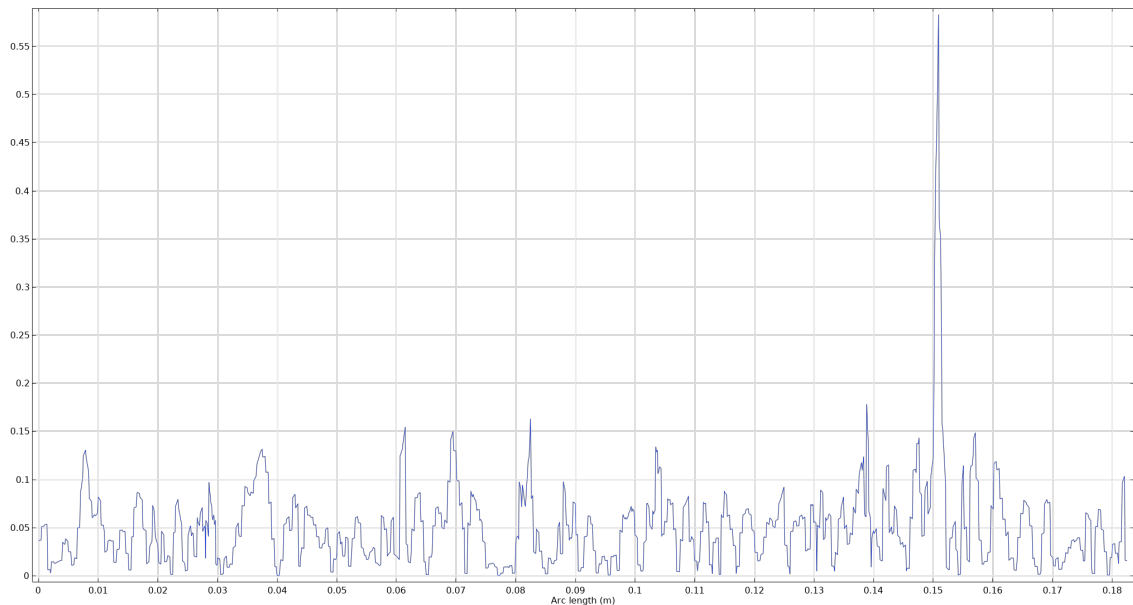


Figure 4-8. Aperture distribution on the outlet of the deformed void space in the Nearing Contact Model. On the x-axis is the distance (in m) from the corner point between Face 3 and 4 to the corner point between Face 4 and 1. On the y-axis is the aperture (in mm) based on the minimum distance to the other edge.

4.2.2 Departing Contact Model

Surface plots

With the *Departing Contact Model*, the aim was to decrease the contact offset towards 0.035 mm. The contact modelling approach with the initial overlap between the rock parts solved much faster than the *Nearing Contact Model*. With 0.1 mm and 0.5 mm contact offsets, a solution was reached in approximately 6 hours. Smaller contact offset values, including 0.035 mm, were also successfully modelled with the contact modelling, but all of them produced geometrical overlap between the parts, preventing fluid flow modelling. The fluid geometry was created from the void space after the final iteration of the contact model, and COMSOL's inbuilt converter could not create it if the overlaps were present. The overlaps were very small and narrow and thus they were not identified as separate geometrical overlap during the geometry sequence. When a mesh is created with the void space geometry containing the small overlap, errors occur in areas of overlap.

Due to overlap in the 0.035 mm contact offset case, visualisation of results are only presented for 0.1 mm and 0.5 mm contact offset runs. The contour of von Mises stresses under 1 MPa normal load in the contact model for both is presented in Figure 4-9 with a colour range similar to the contact pressure film results in the Task Description. In Figure 4-10, the stresses are again plotted, but the colour range corresponds to the UCS of the rock.

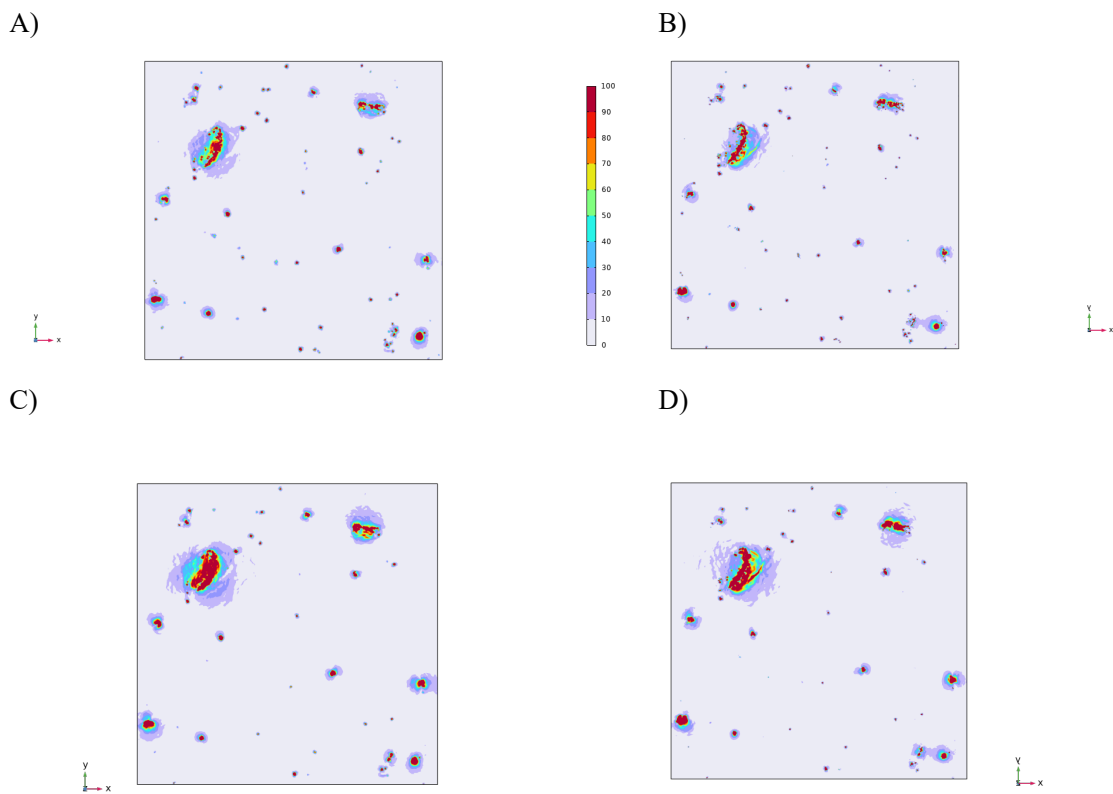


Figure 4-9. von Mises stresses on the top and bottom fracture surfaces. A) bottom fracture surface with 0.05 mm contact offset, B) top surface with 0.05 mm contact offset, C) bottom fracture surface with 0.1 mm contact offset, D) top surface with 0.1 mm contact offset.

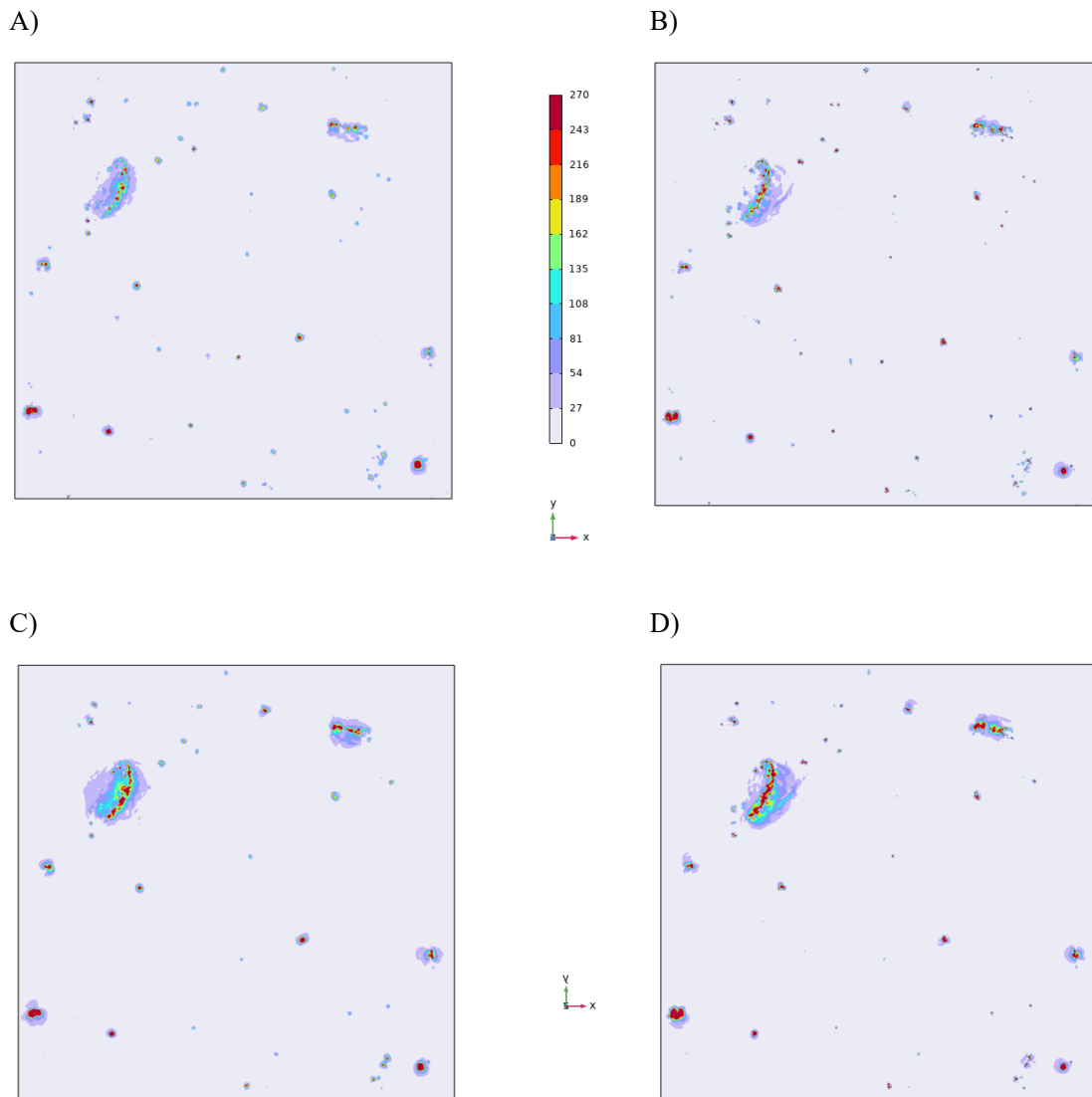


Figure 4-10. von Mises stress on the top and bottom fracture surfaces with the UCS of the rock as the upper limit of the colour range. A) bottom fracture surface with 0.05 mm contact offset, B) top surface with 0.05 mm contact offset, C) bottom fracture surface with 0.1 mm contact offset, D) top surface with 0.1 mm contact offset.

With the *Departing Contact Model*, it was possible to model higher normal loads on the top rock surface within reasonable calculation times. In Figure 4-11 normal loads corresponding to the unloaded case (weight of the top rock part compresses the surfaces to each other), 1, 2, 4, 6, and 8 MPa are presented when using a 0.1 mm contact offset.

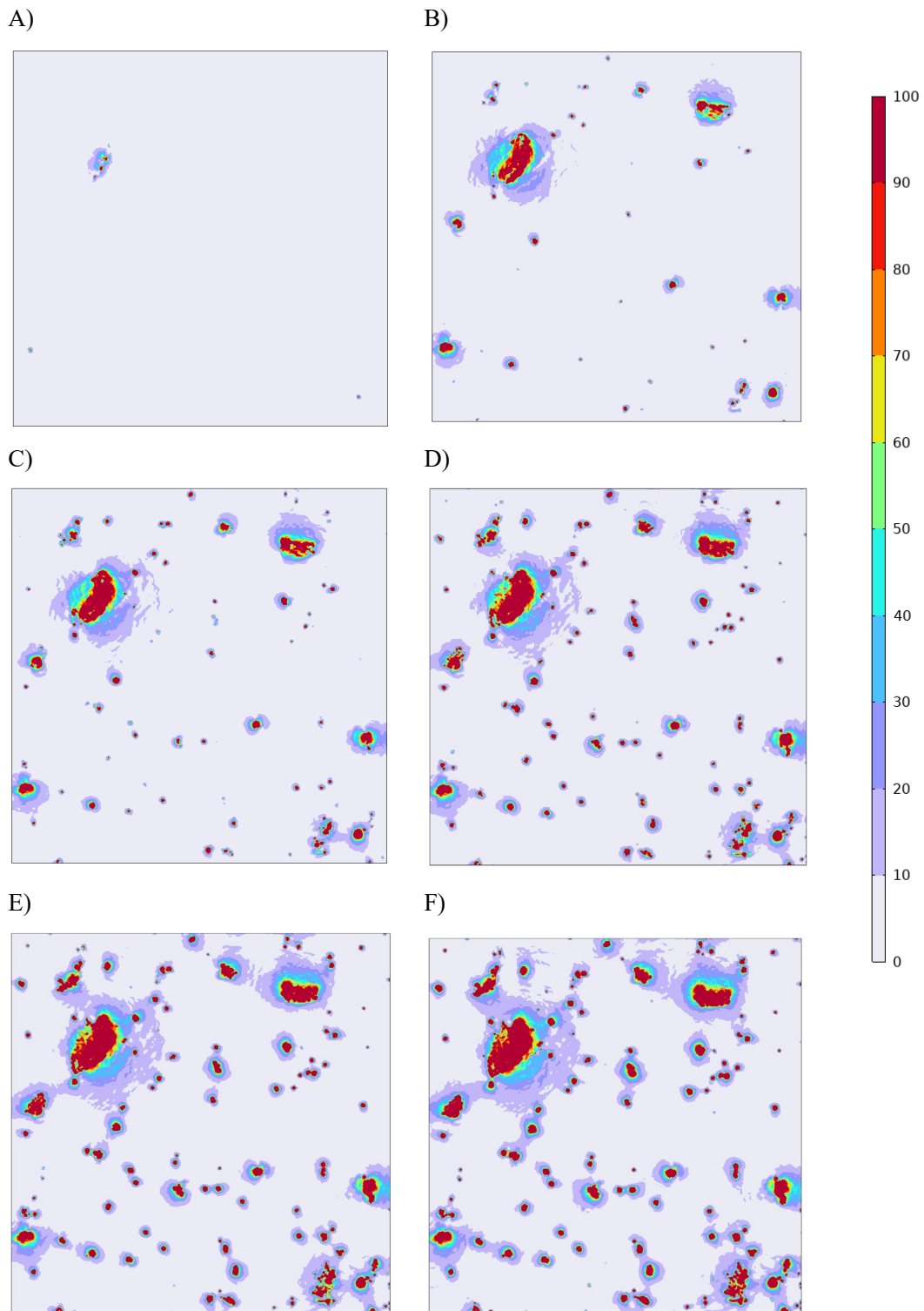


Figure 4-11. von Mises stress (MPa) on the bottom rock surface using Departing Contact Model with a 0.1 mm contact offset value. A) 0 MPa normal load (weight of the rock), B) 1 MPa normal load, C) 2 MPa normal load, D) 4 MPa normal load, E) 6 MPa normal load, and F) 8 MPa normal load. The scale was determined based on the scale used in the pressure film measurements in the Task Description.

In Figure 4-12, the simulated data is compared with the experimental pressure film tests under 4 MPa boundary load and 0.1 mm contact offset. There are only a few distinct contact points in the simulated data, but the pressure film tests seem to record much more widely spread contact areas. This is likely at least partly due to the added film material to the fracture, which is softer than the rock. It can also be noticed that the largest contact area in the simulations (middle of right bottom quarter) corresponds to the white area in the pressure film tests (no contact). This indicates that a piece of rock has fallen off from that particular point after the surface scan, but before performing the pressure film test.

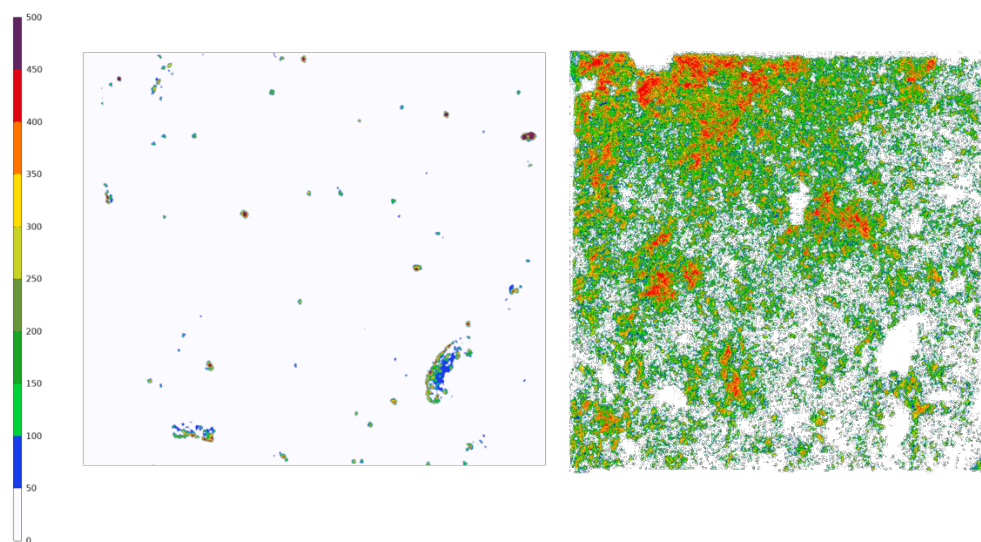


Figure 4-12. Comparison between the experimental pressure film results in MPa (right) and the simulated results using 4 MPa normal load (left).

LVDT data

In the POST experiment, displacements of the rock during the compression tests were monitored with Linear Variable Differential Transformers (LVDTs). Their length after the opening of the fracture was 147 mm and they were placed 200 mm apart in the direction of the flow and 320 mm perpendicular to it. In the *Departing Contact Model*, points that allowed comparison of displacements were defined. As only z-directional movement was allowed in the model, the displacement was calculated as the average of four points on the edges of the sample.

Detailed positions of the LVDT contact points to the rock in the z-direction of the rock sample were not given in the data description. Thus, the LVDTs were placed in the model symmetrically such that the top point was 51.5 mm below the top of the sample and the bottom point 51.5 mm from the bottom. According to this setup, the distance between the points is the LVDT length in the experiment. The LVDT's are placed such that the fracture lays approximately in the middle between their end points.

The data of the points used for calculation of the displacement in the model and the corresponding displacements are presented in Table 4-3. The displacement is calculated as the difference between the average displacement of the four top points and four bottom points. The LVDT data has been zeroed to the 0.02 MPa normal load case. In addition, a value was calculated, where 0.15 mm was subtracted from the modelled displacement values. This was performed to allow easy comparison of the trend of the modelled displacements to the experimentally measured ones in Figure 4-13.

Comparison between the predicted and experimental LVDT displacements are presented in Figure 4-13.

Table 4-3: Displacement values in mm from Departing Contact Model. The force corresponds to the normal load in MPa and the displacement is zero with zero force. The points P1x correspond to edge points above the fracture while points P2x correspond to those below the fracture. P1avg and P2avg are the average displacements of the four upper and lower points correspondingly. Davg is the total displacement between the upper and lower points. Dadj is the total displacement adjusted with 0.15 mm.

Force	P11	P12	P13	P14	P21	P22	P23	P24	P1avg	P2avg	Davg	Dadj
0	0.000	0.000	0.000	0.000	0.000	0.000	0.000	0.000	0.000	0.000	0.000	
1	-0.14	-0.14	-0.14	-0.14	-0.001	-0.001	-0.001	0.000	-0.14	-0.001	-0.14	
2	-0.16	-0.16	-0.16	-0.16	-0.001	-0.002	-0.002	0.000	-0.16	-0.001	-0.16	-0.01
3	-0.17	-0.17	-0.17	-0.17	-0.001	-0.002	-0.002	-0.001	-0.17	-0.002	-0.18	-0.03
4	-0.18	-0.18	-0.18	-0.18	-0.002	-0.003	-0.003	-0.001	-0.18	-0.002	-0.18	-0.03
5	-0.19	-0.19	-0.19	-0.19	-0.002	-0.004	-0.003	-0.002	-0.19	-0.003	-0.19	-0.04
6	-0.20	-0.20	-0.19	-0.20	-0.003	-0.005	-0.004	-0.002	-0.20	-0.003	-0.20	-0.05
7	-0.21	-0.20	-0.20	-0.20	-0.003	-0.01	-0.005	-0.002	-0.20	-0.004	-0.21	-0.06
8	-0.21	-0.21	-0.21	-0.21	-0.003	-0.01	-0.01	-0.003	-0.21	-0.004	-0.22	-0.07

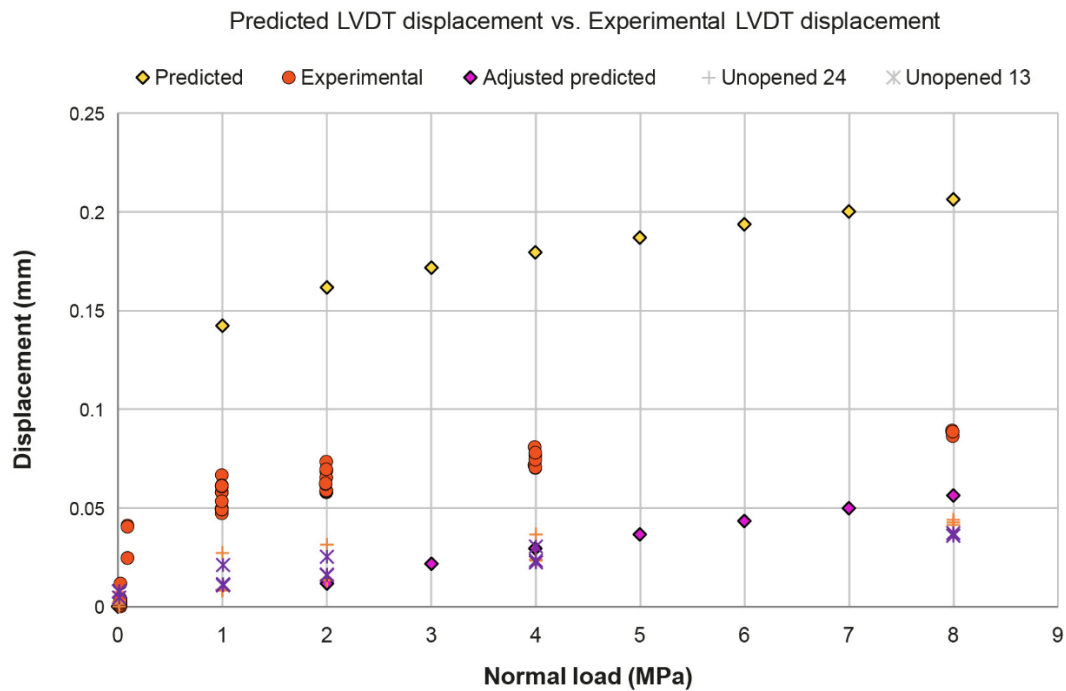


Figure 4-13. Comparison on how the normal load affects the LVDT displacement between the predicted values and the experimental values. The yellow diamonds correspond to the predicted values, the magenta diamonds to predicted values that have been adjusted by -0.15 mm, the red circles correspond to the experimentally determined values after the opening of the fracture in the 24 direction, the orange plus-symbols to experimental values of the unopened fracture in the 24 direction and the purple crosses to experimental values of the unopened fracture in the 13 direction.

The channelling factors and flow rates were again calculated using Equations (18) and (19), and results of the *Departing Contact Model* using different contact offset values are summarised in Table 4-4. The aperture distributions of both contact offsets are presented in Figure 4-14. The average aperture on the outlet boundary was 0.072 mm for the 0.1 mm contact offset and 0.064 mm for the 0.05 mm offset value.

Table 4-4: Results of Departing Contact Model.

Contact offset (mm)	Flow rate (ml/s)	Channelling factor
0.1	90	0.8
0.05	50	0.8
0.035	Overlap in contact formulation	-

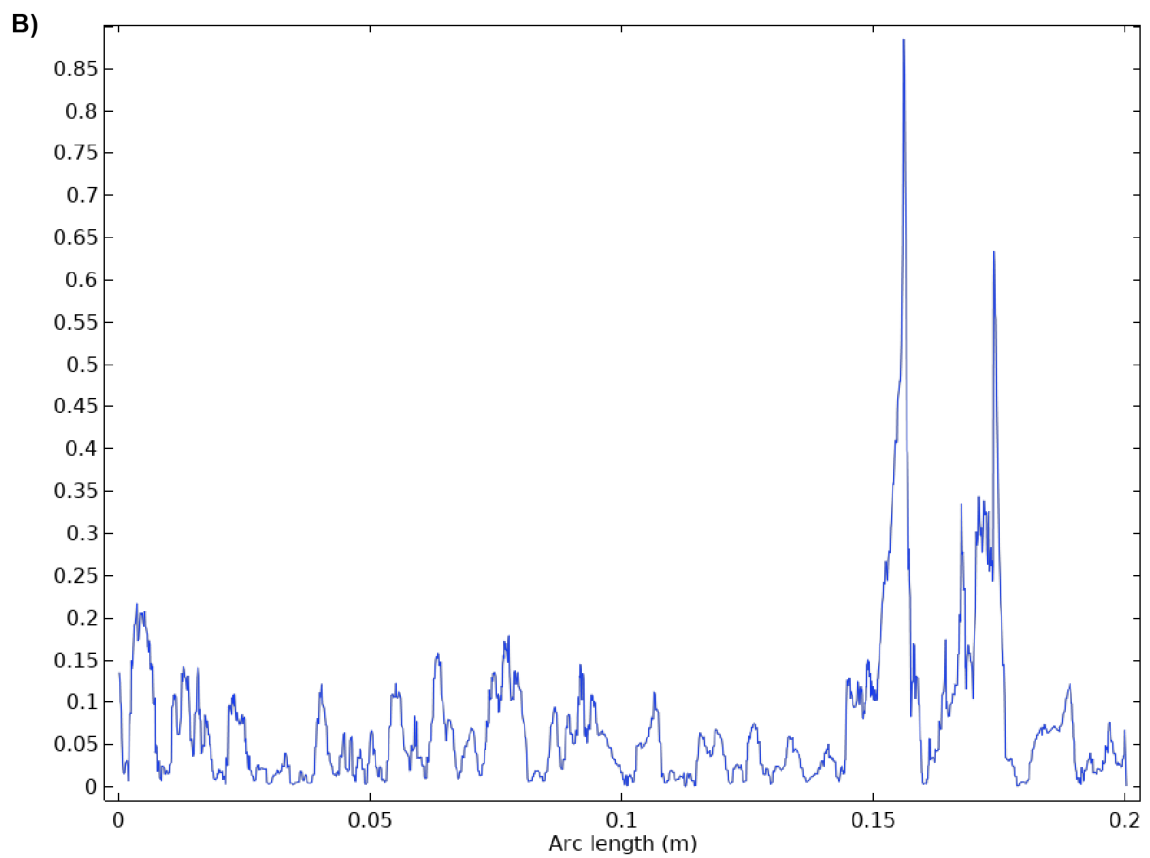
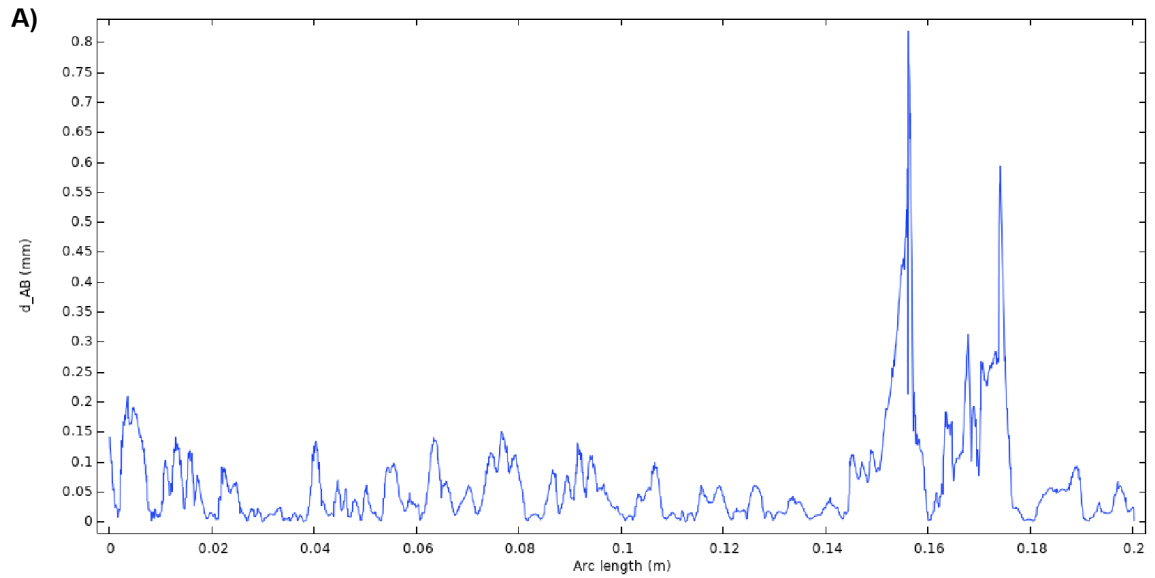


Figure 4-14. Aperture distributions on the outlet of the flow geometry. A) aperture distribution of the 0.05 mm contact offset B) aperture distribution of the 0.10 mm contact offset.

In addition to the flowrates determined with different contact models and contact offset values, the *Departing Contact Model* was used to predict flowrates with different normal loads. The results are presented in Figure 4-15.

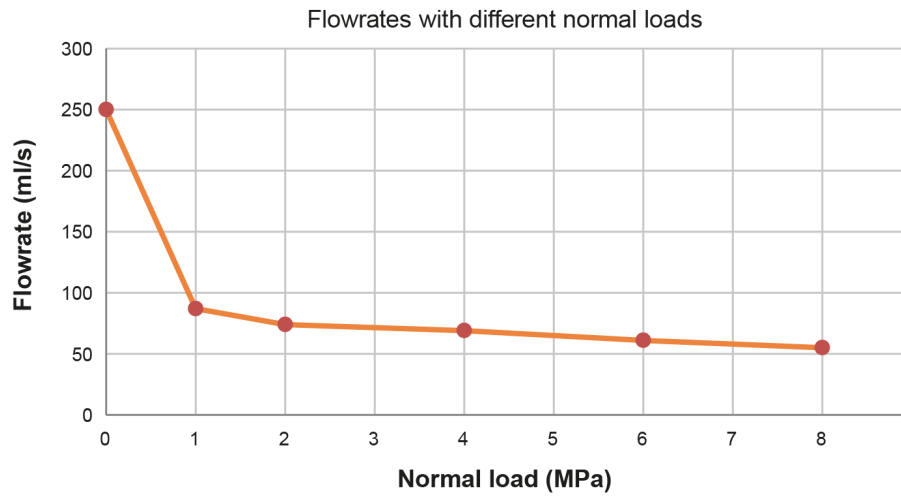


Figure 4-15. Flowrates in ml/s with different normal loads in MPa.

4.3 Experimental results and inverse calculations

Experimentally measured flow rates with 1 MPa boundary load (Table 4-5) were used for inversely calculating effective apertures with the *Analytical Model*. This is the lowest non-zero boundary-load value which presumably results to highest flow rates of the loaded cases, which in turn results in the largest apertures for comparison with surface scan precision.

Table 4-5: Experimental flow rates under 1 MPa of normal load.

A	P in (bar)	P out (bar)	F (kN)	P (MPa)	Flow rate (ml/s)
13	0.265	0.071	39.8	1.00	0.024
14	0.215	0.071	39.8	1.00	0.013
15	0.164	0.071	39.8	1.00	0.007
16	0.115	0.071	39.8	1.00	0.003
28	0.414	0.070	39.8	1.00	0.012
32	0.489	0.071	39.8	1.00	0.029
33	0.438	0.071	39.8	1.00	0.025
43	0.488	0.070	39.8	1.00	0.008
44	0.512	0.071	39.8	1.00	0.008
50	0.512	0.071	39.8	0.99	0.004
51	0.512	0.071	39.8	1.00	0.003
53	0.489	0.071	39.7	0.99	0.009

If Equation (5) is solved for d , the analytically required aperture to reach the experimental flow rates can be calculated:

$$d = \sqrt[3]{-12 \cdot \left(\frac{\partial x}{\partial p}\right) \cdot \mu \cdot \frac{Q}{W}} \quad (22)$$

Assuming a viscosity of 0.001 Pa·s and a void space length and width of 0.2 m, the calculated apertures are summarised in Table 4-6:

Table 4-6: Analytically calculated effective apertures that would correspond to the measured flow rates.

p_{in} (bar)	p_{out} (bar)	Q(ml/s)	d(mm)
0.265	0.071	0.024	0.025
0.215	0.071	0.013	0.022
0.164	0.071	0.007	0.021
0.115	0.071	0.003	0.020
0.414	0.07	0.012	0.016
0.489	0.071	0.029	0.020
0.438	0.071	0.025	0.020
0.488	0.07	0.008	0.013
0.512	0.071	0.008	0.013
0.512	0.071	0.004	0.010
0.512	0.071	0.003	0.009
0.489	0.071	0.009	0.014

5 Discussion and conclusions

5.1 Discussion

As is evident from the results, the numerically predicted flow rates in the contact models are significantly larger than the experimentally measured ones. In this section, the results of all five models and possible reasons for the difference with the experimental results are discussed.

5.1.1 Analytical solution

To analyse the effect of fracture surface scan precision uncertainty on the flow rate, the flow rate in a smooth fracture with an effective aperture corresponding to the fracture surface scan precision (0.035 mm) was calculated. In principle, a zero (pointwise) aperture between the upper and lower fracture surfaces in the model could still mean an aperture of the measurement precision in reality (if the distance between two points is less than the measurement precision, they can be either on top of each other, the distance can be the measurement precision, or something between).

As seen from Table 4-1, the flow rate corresponding to the measurement precision of 0.035 mm is 0.1 ml/s, which can be considered as an estimate for the error in the simple flow model due to the surface scan precision uncertainty. Since the measured flow rates are on this order of magnitude, the surface scan precision can be considered to be not enough to allow meaningful modelling of water flow between the fracture surfaces with such low flow rates.

After the experimental flow rate results were published, the *Analytical Model* was also used to inversely calculate the effective apertures with which the experimental flow rates are reproduced. As can also be seen from the back-calculated results in Table 4-6, the analytically calculated apertures required to reproduce the flow rates are all below the model scanning precision. There is scatter in the experimental flow rate results, but, for example, the aperture in the *Analytical Model* needed to reproduce a flow rate of 0.012 ml/s should be 0.016 mm. Consequently, the fracture scan measurement precision should be less than this aperture to be able to produce a model with the surface scan data that could reproduce the flow rate accurately.

5.1.2 Parallel Plate Model

The *Parallel Plate Model* successfully reproduced the flow rates by the *Analytical Model*. Flow rates in the model are negligibly smaller than in the analytical predictions, likely due to numerical errors resulting from the current mesh density. Nonetheless, the accuracy was considered enough for the subsequent flow modelling. While the results of the *Parallel Plate Model* are not utilised for the later models, its objective of being a bridge between the analytical and numerical model was met. It also further shows that with an aperture corresponding to the surface scan precision (0.035 mm), the flow rate is an order of magnitude larger than the average experimental results using a 1 MPa normal load.

5.1.3 Small Surface Model

The sensitivity analysis showed that deviations in the x-, y-, and z-placement of the top surface have a statistically significant influence on the flow rate. Out of the three, z-directional deviations have the largest impact. Rotations around the z-axis were not influential.

For the contact models, this would mean that in addition to the z-directional movement of the rock sample, also movement in the horizontal directions should be allowed. For now, the model does not allow such movement. Horizontal movements can cause the fracture surfaces to interlock at a lower level (which means smaller aperture) in comparison to the case where they were modelled. This could lead to smaller flow rates than the predicted ones.

The procedure developed for the sensitivity analysis with the *Small Surface Model* could be used for conducting similar sensitivity analyses with a higher number of input parameters and with more complicated models (that was aimed at with the contact models). The process can be fully automated once a reliable numerical model has been created. During the sensitivity analysis, the COMSOL Multiphysics model was operated by connecting it to Matlab. This way, the DoE could easily be incorporated in the model workflow so that changes in the top surface placement could be read from a file and used to change the model geometry. With the *Small Surface Model*, the numerical solutions were also fast, allowing for a reasonable total computational time when performing the DSD method.

5.1.4 Contact models

Developing the contact model was a long process. The methodology was initially developed with the smaller fracture surface scans delivered for Task 10.2.1 (see the Task Description). With the smaller surfaces, the required computational effort was lower, and solutions converged relatively fast with good stability. This methodology was used as the basis for the larger sample of Task 10.2.2. The first results were computed with an older model that was based directly on the fracture surface scan data (without the clipping areas removed). This caused the aperture of the deformed void space to be much larger than anticipated, resulting in a flow of nearly 1 l/s.

After the clipping areas were removed, the model failed to converge. Multiple revisions were performed, and after discussions with contact modelling experts, the problem seemed to be the lack of mesh density. The mesh density was increased, and the first results after the removal of the clipping areas were obtained with a calculation time of over three weeks. However, successful model convergence acted as a proof of concept that the methodology could be used for the flow rate prediction. The model was updated to use the provided material parameters and the final version of the *Nearing Contact Model* was created.

Nearing Contact Model

The new approach successfully converged so that a solution to the contact problem could be obtained. The resulting deformed model geometry was also successfully converted into a flow geometry without problems with geometric overlap of the fracture surfaces (geometric overlap is discussed below in detail).

A contact offset of 0.1 mm was used in most of the contact model simulations. During the model development, this value resulted in deformed fracture geometries that could be used easily in the subsequent water flow modelling. When the order of magnitude of the experimental flow rates (measured in drops) were discussed the first time (before releasing the measured data), the effect of the already made choices in modelling and inherited model features (including the contact offset and the fracture surface scan precision) on flow rates were further investigated. Both of the contact offset and the scan precision turned out important for the slow flow rates.

From the *Analytical Model* results, it can be seen that a contact gap of 0.1 mm contributes approximately 2.6 ml/s to the flow (if the contact gap is used as the effective aperture). While the usage of the effective aperture is crude and does not consider heterogeneous apertures, it is a useful way to better understand the effect of the contact gap and allows the effect to be compared with other contributors to the total flow rate. The flow rate is higher than the analytically determined flow rate corresponding to the fracture scan precision, which gave an error estimate of 0.1 ml/s to the predicted flow rate. This meant that a smaller contact offset was required to bring the error to a comparable level. Thus, our modelling team decided to run the model with a smaller contact offset of 0.035 mm. Unfortunately, the model did not converge to a solution. Presumably a denser mesh would be needed to solve the problem but increasing the mesh density was not practical. Due to the long computational times with the *Nearing contact Model*, adjusting the model was impractical, which ultimately led to the creation of the *Departing Contact Model*.

Later, when the results of the POST experiment were published, it was clear that our model had failed to predict the flow rates. The flow rates using both contact modelling approaches were orders of magnitude higher than the results obtained from the experiment. With the contact models, the flow rates range was on the order of 100 ml/s depending on the approach, while the rate under a 1 MPa normal load was on the order of 0.01 ml/s in the experiment. The effect of the contact offset does not explain the deviation from the experimental values, as it only accounts for approximately 3 ml/s of the total modelled flow rate as discussed above. Thus, a too large total aperture (including the real aperture and the contact offset) of the deformed void space could be the reason. The average aperture was 0.05 mm with the model, which also only yields a rate of 0.33 ml/s if the flowrate is calculated with *Analytical Model* (cubic law) using the average aperture as the effective aperture. However, for the aperture distribution in Figure 4-8, a section with a very large aperture of approximately 0.6 mm is visible. If the whole fracture in the experiment would have 0.6 mm effective aperture, the flowrate would be close to 600 ml/s if calculated with the cubic law. It is possible that, for example, connected areas like this in the fracture contribute greatly to the calculated flow rate.

The large aperture could be possibly explained by the modelling of rock deformation. In our approach, deformation was considered elastic. If the permanent deformation would be modelled, the rock could be damaged in areas of high stress concentrations, resulting in a smaller aperture. Furthermore, the clipping of the overlap present in the provided fracture surface scan data also increases the contact area between the top and bottom surface, as the clipping ensures that in the affected areas the surfaces align. This increased surface area for contact also decreases the deformation in the rock parts, resulting in a larger compressed aperture elsewhere. However, when the LVDT and pressure film data is compared, it can be seen that less contact points exist in our model than in the pressure film and the initial deformation in the unloaded case is larger than in the experiment. This indicates that due to less contact points the smallest points deform initially more and then the deformation slows down maybe due to the trimmed contact areas. In the unloaded case, it could also be possible that the fluid pressure has an effect on the flow rates, but this was not addressed in this study.

Departing Contact Model:

With the *Departing Contact Model*, convergence of the contact model using a similar contact offset of 0.1 mm was achieved much faster than with the *Nearing Contact Model* (in approximately 6 hours). This proved to be a good starting point in reaching the contact offset target of 0.035 mm.

While the contact model converged using the gap offset value of 0.035 mm, creating a subsequent void space model was not possible due to small overlaps in the geometry. The overlap is discussed later in this section.

Nevertheless, the approach was successful in creating the geometry for the fluid flow modelling using offset values of 0.1 mm and 0.05 mm. When von Mises stress distributions on the surfaces are compared between the *Nearing contact* and the *Departing Contact Models*, it can be seen that stress concentrations are not identical but located roughly in the same areas. Although the contact modelling approaches should yield similar results, the differences likely originate from the errors related to the approaches and the representation of the geometry in the model. In the *Nearing Contact Model*, the spring is gradually made weaker, and the deformation on the surfaces is iteratively changing throughout the process. In the *Departing Contact Model*, no iterations between different spring strengths are used, and a deformed configuration is solved for immediately.

Similarly to von Mises stress distributions, the different contact model approaches result in differences in the outlet aperture distributions. In the *Nearing Contact Model*, a larger aperture (approximately 0.6 mm) is near the corner point between Face 1 and 4. This aperture is also present in the *Departing Contact Model*, but the aperture is somewhat different (approximately 0.85 mm). The average aperture is also smaller with the *Nearing Contact Model*. However, when the flow rates are compared, the flow rate with the *Departing Contact Model* is smaller with both contact offsets. This would indicate that the overall aperture with the *Departing Contact Model* is smaller than with the *Nearing Contact Model*. The reason for the difference between the models is not clear and would require further investigations.

When the predicted flow rate was compared with the experimental results, it was again evident that the prediction had failed. The flow rates were significantly larger than the experimental values. The underlying reasons are similar as discussed for the *Nearing Contact Model*.

In summary, the *Departing Contact Model* was much faster at solving the contact problem and thus could be used for faster model development. With a larger contact offset value, the approach was able to produce a working flow model. However, the flow rates were again significantly larger than the experimental values, indicating that the deformed aperture was again larger than in the experiment. Furthermore, the goal would be to decrease the contact offset so that its effect would be negligible. In the *Departing Contact Model* smaller values lead into overlaps in contact geometry preventing the creation of the flow geometry altogether.

Pressure film results

As can be seen from the comparison of the experimental pressure film data and the predicted results (Figure 4-12), the area under contact is much less in the predicted results. This could be partly explained by the thickness of the pressure film interacting with the fracture surfaces showing contact pressures in areas where there would be no contact without the film.

More interestingly, however, is the fact that the areas with the highest contact pressure in our model are roughly situated in white spots of the contact film. In the film results, this means that no contact exists between the top and bottom rock part. The same areas also correspond to the sections of initial overlap in the surface measurement data in Figure 3-7. In the Task Description, it was also discussed how the opening of the fracture was not spontaneous and a considerable force was needed. After the fracture opening, some rock parts had chipped away. As the same areas have simultaneously overlap in the surface scan data and no contact in the pressure film results, we assume that the surface scanning was conducted before all the chipped or loosened rocks were removed, that is, some chipped parts were included in the scan, presumably since they were not completely loose and not noticed during scanning. Thus, in the pressure film data, the areas without contact that overlap with the high contact pressure areas of the model would be areas where rock has fallen out. Verifying this would mean going back to the experimental data. One option would be that another surface scan would be conducted so that both the current and the updated surface scan dataset could be compared to assess whether our assumption is true or not. It is not clear if this would be possible after the loading test with high normal loads performed at the late stages of the experiments.

LVDT data

The comparison of the LVDT data to the simulations is carried out without exact information about the initial fracture aperture. Although the initial placement of the top and bottom rock parts was measured and fracture surfaces were scanned, the inability to simulate the experimentally measured flowrates led to a conclusion of high uncertainties in the fracture aperture. Consequently, the experimental relative displacement data is compared to the modelled relative displacement results. Therefore, dimensionless measures of deformation (such as strain) cannot be used and comparison, for example, of rock mechanical parameters (e.g. Young's modulus) cannot be performed.

As seen from the comparison of the LVDT and predicted data in Section 4.4, the displacement in the model is larger in comparison to the experimental data. This is especially evident in the unloaded case and the 1 MPa normal load case, where the displacement in the model was almost 0.15 mm, whereas the measured displacements were between 0.01 mm and 0.07 mm depending how many loading-unloading cycles have been performed. When the displacements of the higher loads (from 2 MPa onwards) are compared, it can be seen that the trend of the predicted data aligns quite well with the experimental results (adjusted modelling results, where 0.15 mm was removed from all displacements vs experimental results), although the trends are slightly different (modelled displacements increase faster with the normal load than the experimental ones). The larger displacements in the model at low loads indicates that our model has less contact points initially than the real fracture surfaces which causes the rock at the contact points to deform more under low loads than the real rock parts (smaller area carrying the normal load means more deformation). This is in line with the comparison of the modelled contact points to the pressure film data. When compressed with a sufficiently high load, the displacement increase per normal load increase in the model is close to the experimental findings. This suggests that the real contact area is better captured by the model at these higher loads, even though the mechanical constitutive model is only linear elastic and lack the rock breaking or yielding mechanisms.

Another aspect that could affect the unloaded case is the omitted effect of water pressure during compression in the model. In the experiment, the water pressure applied to the sample resists the normal load somewhat, whereas in our model it does not. Investigating the effect of this is outside the scope of this study.

Overall discussion on the contact model approach

As was discussed earlier, overlap in the contact model creation was a major issue preventing the creation of the subsequent fluid flow model. Two types of overlap can occur. The first type results from the imperfect contact models and is hereinafter called *geometric overlap*. The second type results from poor meshing of the flow model (subsequent to contact modelling) and is hereinafter called *meshing overlap*.

In the contact models, the normal load applied on the top rock part forces the two rock parts in contact to each other. In the *Nearing Contact Model*, the contact formulation aims to prevent the top part from overlapping with the bottom rock part when the spring constant described in Section 3.1.2 is decreased. Similarly, in the *Departing Contact Model*, the contact formulation aims to move the top rock part out of the bottom rock part to remove this initial overlap. With the contact formulation, the stress state and resulting rock deformation are calculated, and in an ideal case, no overlap remains between the rock parts. Often the primary objective in contact formulations is, however, to model the mechanical behaviour of the contact (for example, for the wear of the surfaces in contact) and perfect separation of the contact surfaces is not needed. With this respect, different contact model formulations result in varying amounts of overlap between the surfaces in contact. From the three predefined contact formulations in COMSOL Multiphysics (COMSOL, 2022a), the penalty method (penalty function for the overlap, but no perfect separation of the contact surfaces) results in the most overlap but is also computationally least expensive. The Augmented Lagrangian contact method is claimed to produce the least amount of overlap, but it is not perfect at unless very dense meshes are generated. The third method, the Nitsche method, is somewhere between the two other methods, but the tests with it produced too much overlap for creating the flow model geometry, although it was computationally less expensive than the Augmented Lagrangian method. The remaining overlap with the current meshes and with the Augmented Lagrangian method (which was used in the contact modelling) was on the order of 0.01 – 0.1 mm. This overlap is visualised in Figure 5-1.

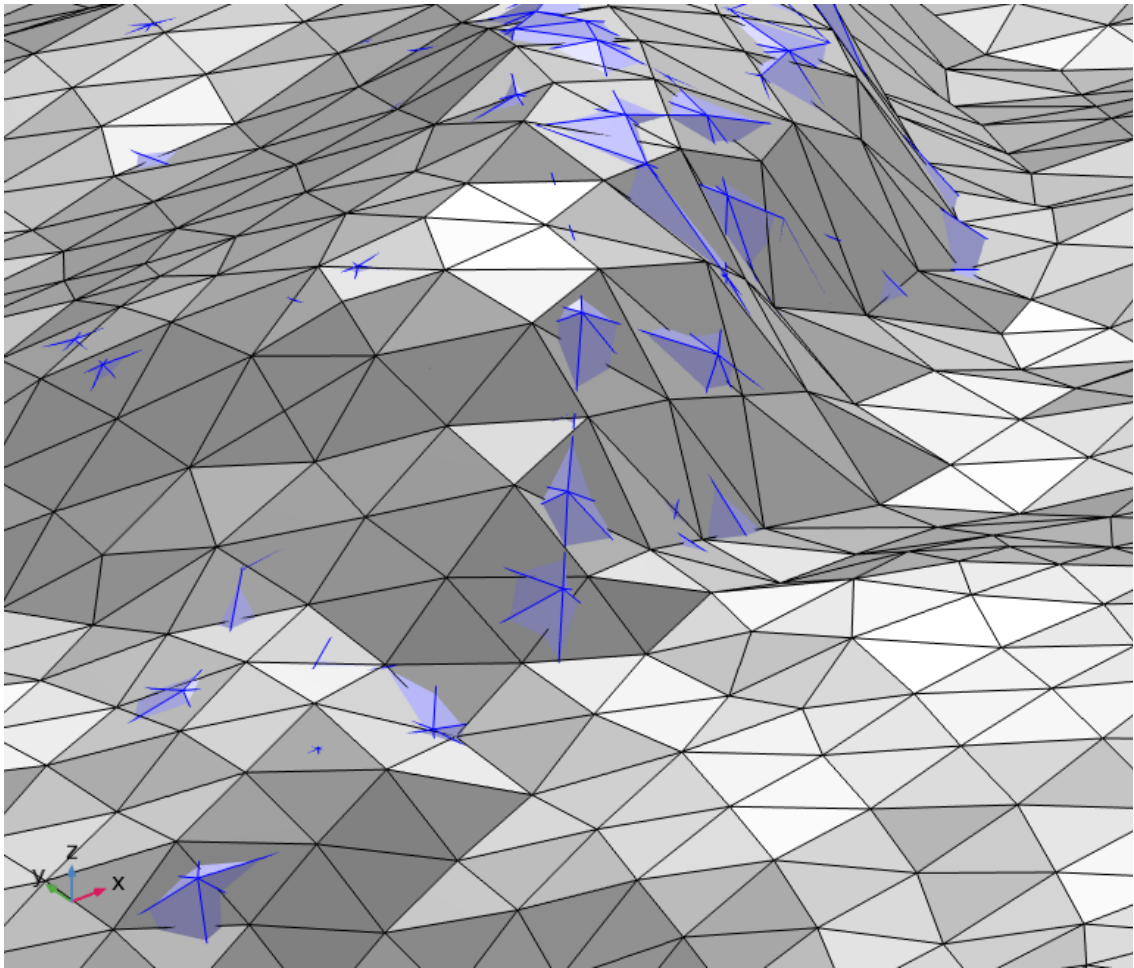


Figure 5-1. *Overlap between the bottom and top fracture surfaces. It can be seen how the lower fracture surface penetrates the upper one. This overlap can be either due to geometric overlap in the contact modelling or due to an insufficient mesh density.*

To prevent the overlap altogether during the contact modelling, a contact offset can be applied as presented in Equation (13). This causes the contact formulation to activate contact before the surfaces are in geometric contact and forces a small gap between the surfaces. If a sufficiently large offset value is used, all geometric overlap can be prevented with reasonable mesh density, as seen in Figure 5-2. However, as discussed in Sections 4.1 and 5.1.1, this added offset also influences the flow rate. Thus, a compromise between a sufficiently small contact offset and prevention of geometric overlap must be made.

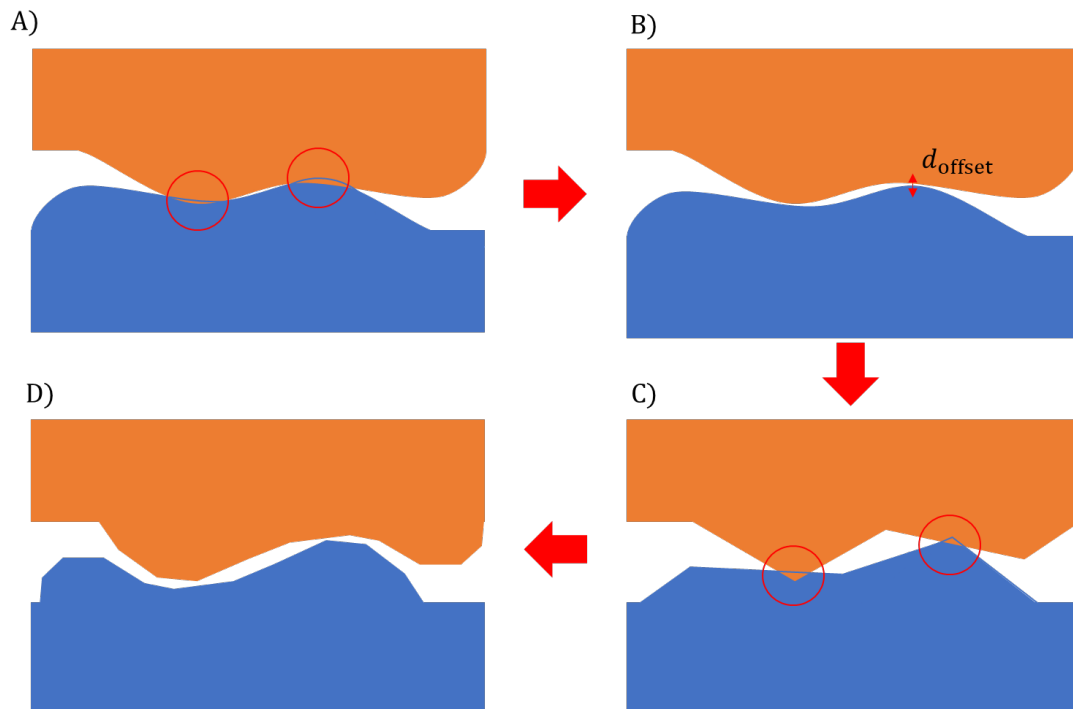


Figure 5-2. Representation on how geometric or mesh overlap can occur. A) In the contact model, the contact formulation aims to prevent overlap between the two rock parts under compression. Some small overlap is still possible, where one surface penetrates the other. B) A small contact offset (d_{offset}) can be used to prevent this geometric overlap. C) When the resulting domains are re-meshed for the flow rate model, meshing overlap due to too low mesh density can occur. D) This meshing overlap can be removed by using a denser mesh.

Even if the geometric overlap can be prevented, overlap can also occur when the deformed configuration is meshed (meshing overlap). This can occur if the mesh of the deformed geometry is not sufficiently dense. If the surface has a lot of unevenness or undulations, as is the case with many fracture geometries, the undulations are smoothed out with a coarse mesh and overlap on the mesh boundary elements can occur (visualised in Figure 5-1 and Figure 5-2). This overlap can be prevented by using a denser mesh as presented in Figure 5-2. Then again, a denser mesh requires more computational capacities when used in the numerical model. Thus, a compromise between mesh density and available computational resources needs to be made.

As a summary, the contact model approach suffers from the inherent limitation of geometric overlap with geometrically complicated fracture surfaces unless impractically dense meshes are used and, thus, a contact offset is needed in practice to avoid overlap. If the flow rate in a fracture is sufficiently high, the relative error made by including the contact offset is small. If the flow aperture is small and, thereby, the flow rate low, the error due to the contact offset may become significant. With the low flow rates in the experiment modelled here, it is crucial to aim for as low an offset as possible, but this requires also a very dense mesh which, in turn, leads to high computational costs to run the contact models. With very slow flow rates in fractures with small apertures, the influence of the added contact offset to the aperture may cause ten times higher modelled (with cubic law) flow rates than experimentally measured rates. The backwards calculations with the *Analytical Model* in Section 4.5 show that an offset in the range of 0.02 – 0.03 mm or below would bring the added flow rate into the same magnitude as the flow measured in the experiment. If the water flow in the POST experiment fracture is considered, the offset would need to be even smaller to have a reasonably small error due to it. Reaching such small offset would lead to impractical computational effort and time requirements.

In addition to the problems with the contact offset, the rock mechanical model should be developed further. In the view of the LVDT relative displacement comparison, the linear elastic model produces surprisingly similar displacement as measured with high normal loads, but the model does not capture the observed remaining permanent deformations resulting from the experimental loading-unloading cycles. This would be needed to better understand the rock mechanical behaviour (e.g. when the rock breaks) and to further validate the rock mechanical model, but the effect on the water flow rate modelling is likely small in comparison to other effects discussed above. The effect on flow channelling could be significant if the flow rates would be close to the experimentally measured rates.

The overlap of the scanned fracture surfaces when virtually placed on top of each other according to their measured positions suggests that the uncertainties related to the rock behaviour during opening the fracture are high. The overlap indicates that the rock breaks likely under tensile stresses that result from using force when opening the fracture. During the process, extra void volume in form of new cracks and fractures within the rock is created (corresponding to the overlapping rock volume). In our models, this extra void space is removed straightforwardly with the clipping process (Section 3.1.2) and no alteration in the rock mechanical properties are considered (the elastic parameters are the same and permanent deformation models are not considered). Consequently, the contact of the fracture surface becomes perfect on the clipped, relatively large areas, which may cause the rock to behave stiffer during the compression than it does in the experiment. Besides the simplified model describing rock behaviour during compression, the effect of uncertainties in fracture surface geometry due the fracture opening process and the consequent modelling choices on the initial fracture aperture may be significant. Since the fracture aperture is a deciding factor for the flow rate, the effect on the flow rate may also be significant. The evident problem in reducing this type of uncertainties is that it is difficult to experimentally measure or assess impact of the opening on the rock.

Assuming that the confidence in the rock mechanical deformation model and in the process to handle the fracture surface overlap can be increased, the contact model might be suitable for fractures with larger initial apertures, and consequently larger flow rates, despite the issues with the contact offset. Then the error in comparison to the larger flow rate resulting from the contact offset would be small. For further studies, it is suggested that first the differences between the *Nearing Contact Model* and the *Departing Contact Model* are understood. The latter model is much faster, allowing for a faster model development and adjustment. Thus, it should be ensured that results obtained with the model are justifiable. With the more flexible (faster calculation time and thus easier adjustments between model iterations) *Departing Contact Model*, creating a detailed sensitivity study would be much more sensible.

5.1.5 Discussion of the modelling goals

The first objective was to obtain a better understanding of how the measurement precision and fracture surface placement affects the simulated flow rates. This objective was reached, as the analytical solution and back-calculation of the experimental results gave a general understanding of the equivalent aperture required to reproduce the experimental results in a parallel plate case. This information was then compared with the measurement precision, and it was noticed that the precision was not sufficient to simulate the flow accurately or reliably on a level that would match the experimental results. This is especially problematic with slow flow rates as those observed in the POST experiment.

The sensitivity analyses also showed that deviations in the z-direction are most influential in the fracture surface placement. This is also sensible, as in Equation (6), the flowrate is proportional to the cube of the aperture. Thus, small deviations in the z-direction can lead to large differences in flow rates. For the numerical modelling, this means that the limitation of studying only the z-directional movement of the rock part was justifiable. In a real case, however, the rock could also move slightly in x- and y-directions, and the rock parts could interlock better, decreasing the smaller final aperture after the compression. Such movements could be reproduced in the future by removing the roller boundary conditions from the sides of the upper surface during the normal loading and assigning, for example, some spring-based constraints to guide the movement to a correct position (some constraint is needed to not allow random rigid displacements). Another option would be to model friction between the fracture surfaces under contact. An evident prerequisite for such approaches would be convergence of the elaborated models, which is not guaranteed based on first attempts.

The second objective was to predict the fracture flow rates of the POST experiment during different normal loads using a contact model mimicking the mechanical deformation of the rock especially close to the fracture surfaces. Deformation resulting from contact between the fracture surfaces was modelled successfully using a single normal load (1 MPa) with the *Nearing Contact Model* and using 0, 1, 2, 4 and 8 MPa normal loads with the *Departing Contact Model*. Stress states were obtained, and the workflow from the contact model to a flow model was demonstrated. The fluid flow model produced three-dimensional flow fields, from which flow rates were calculated, but the flow rate predictions were off by several orders of magnitudes. Furthermore, a better understanding of flow channelling within the model was aimed for. Although the three-dimensional flow field can be used to assess the flow channelling, it is likely not captured accurately due to too high modelled flow rates. Consequently, the calculated channelling factors likely do not tell much about the true channelling of the flow in the experiment. It is anticipated that the factors would be lower with smaller fracture apertures due to smaller ratio of open space for flow to near-fracture-surface space where the undulating surfaces obstruct the flow. The major part of the modelling time was used in trying to achieve model convergence in the contact model. Thus, no sensitivity analysis on the contact and fluid flow model results could be performed.

The successful modelling workflow, however, showed that the modelling approach could be used in similar problems in the future. The problems with model convergence, and to a part with the geometrical overlap, were related to the mesh density. If more computational capacities were used, a model with a denser mesh could be created and the modelling approach tried with that. Other options would be to manually or algorithmically remove the overlapping areas in the fracture geometry. The model could also be tried with a smaller model or experimental geometries, as the workflow seemed to work better with the samples from Task 10.2.1. Other, longer-term goals would be incorporating the x- and y- directional movements during the contact problem for allowing the model to better interlock. Permanent deformation of the rock should also be incorporated as it could potentially decrease the aperture after normal load by a great deal.

Overall, the contact modelling exercise was useful, as problems such as the requirement for high computational capacities and the inherent problem regarding the contact offset were identified. If contact modelling is utilized in the future, differences between the two approaches, the *Nearing contact* and *Departing contact models*, should be understood. It also showed that a contact modelling approach might be more suitable for rougher fractures where with large flow rates, where local deformation in the contact points would be large and have a significant effect on the total flow.

5.1.6 Other discussion

Precision of the provided data is another important topic to be discussed. The fracture surface scans have a very high precision, resulting in large, hard-to-work-with data sets, at least for contact modelling. On the other hand, the measurement precision results in a fairly large uncertainty regarding very small modelled flow rates considered in this study.

The first dataset of Task 10.2.1 was used for the sensitivity analysis. With the point density and sample size, the handling of the data, model creation and solving the problem was possible in a reasonable time with a standard computing server. The data set of Task 10.2.2 was larger and, consequently, any modelling steps or processes were slow (including basic operations such as opening files or visualising the data). Our modelling team switched to a more powerful modern computing server, but the simulation times, especially with the *Nearing contact model*, took much wall-clock time. This made it hard to adjust the model and aim for a smaller contact offset. From this perspective, a smaller dataset, for example through a smaller sample in the experiment, could be more pragmatic to work with. It would allow for more iterations and faster model development. In contrast, having less dense data or data with lower quality poses a problem for accurately predicting flow rates.

Despite the dense point cloud that was provided, the surface precision had an influence on the simulated flow rates. As was seen with the results of the *Analytical Model*, the maximum flow rate in a flat fracture with effective aperture corresponding to the measurement precision was higher than the measured rate. This, combined with the inherent property of the contact model requiring a small contact offset, makes it hard to predict flow in fractures with very small apertures. This also means that less data or data with lower quality would negatively affect the results. It would add to the flow rate estimation error making any predictions less reliable. This also supports the suggestion of using smaller samples, with which the resolution of the data could also be higher, yet still having a smaller point cloud size.

To explain the large difference in the modelled and experimental flow rates, the possibility of having an unnoticed issue in the experimental setup was discussed in and after Task Force Meeting #41. One considered possibility to explain such large difference is air bubbles (remaining or formation of them) in the fracture space and the blocking of the flow due to the bubbles. In an email exchange with the Task PI, the protocol to avoid bubble formation was explained and it seemed to be adequate to prevent the issue. After connecting the hydraulic system to the rock sample and applying the pressure gradient, irregular flow occurred for several hours. The irregular flow was interpreted as flushing of the air from the fracture, but steady-state flow was reached, which was considered an indication that the air was removed from the system. The hydraulic system was run usually overnight before making the flow measurements. Moreover, de-gassed water was used to avoid bubble formation during the experiment. Even though these precautions were taken, it is difficult to be certain of not having air bubbles in the system simply because it is difficult to detect them in the rock. It would be of interest to estimate the pressure needed to overcome the capillary forces that may keep the air between the fracture surfaces in the future.

The opening of the fracture due to water pressure in the zero-load case of the hydromechanical POST experiment was suggested possible by one of the other modelling groups. In our modelling this effect was omitted. The force and moment balance calculations (in Appendix A) performed after the modelling confirm that this is indeed possible at least in principle. Based on the calculations, the effect should be so distinct that the instrumentation should have caught that clearly.

5.1.7 Pragmatic validation

The reflection of the success in reaching the validity rank 18 (in Section 3.1.8 according to Section 2.4) yielded the following considerations. It was possible to model the water flow between the fracture surfaces with zero normal load, but the flow rate was off by several orders of magnitudes. Consequently, the parameter n for the flow rate is considered 0.05. With successful validation, the parameter for flow model would have been 1.

The mechanical contact model results were compared to the experimental LVDT data. The trend was somewhat captured with high normal loads, but not that well with low normal loads. The elastic model is, however, not able to simulate the breaking of the rock, which likely occurs in the experiment due to exceeding the uniaxial compressive strength. Moreover, even though only a two-parameter elastic model and unaltered fracture surface geometries were used from previous models, the simulations were run when the data was already available (not a blind prediction). Consequently, the resulting worth of mechanical model validation for the parameter n is considered 0.5 (instead of the aimed 1 for successful validation).

Complicated coupled simulations (where the flow simulation in a deformed fracture void space followed the contact modelling with different normal loads) were performed, but again the flow rates were consistently off by several orders of magnitudes from the experimental values. Consequently, the worth for parameter p is considered 0.05 (instead of the aimed 1 for successful validation).

Altogether, the resulting validation rank is $n \cdot m^{(1+p)} = (0.05+0.5) \cdot 3^{(1+0.05)} = 1.7$. For a flow model only (Example 1 in Section 2.4), the validation rank would be $n \cdot m^{(1+p)} = 1 \cdot 1^{(1+0)} = 1$. Consequently, this suggests, from the validity rank perspective, that the coupled model is better than an only water flow including successfully validated model, but not much. Obvious from the above test run for the calculation of the validation rank, further development of the validation rank definition and the criteria for evaluating its parameters are required, but the format here could serve as a starting point.

5.2 Conclusions

In this study, the modelling approach combining contact modelling and subsequent flow modelling in the deformed fracture was used to predict fluid flow rates between two fracture surfaces under a normal load. The first step of the approach was to simulate the deformation of the rock and fracture surfaces, and the second step was simulating the water flow in the deformed fracture. With the mechanical contact model, it was possible to create deformed three-dimensional fracture void space geometries (within the modelling and the background data accuracy) with multiple contact points under various normal loading. As an example of the resulting fracture apertures, the average aperture on the outlet of the fracture was in the range of 0.05–0.09 mm using the two contact modelling approaches (*Nearing and Departing Contact Models*) under different normal loads. The variation in the aperture distribution was, however, large.

The modelled average displacements between the top rock part (above the fracture) and the bottom part (below the fracture) under varying normal loading were compared to the measured average displacement. With low normal loading (no loading or 1 MPa), the contact model gave larger deformations than the experimental results, but with higher loading (2–8 MPa) the trend of the experimental results was reasonably well captured with the contact model. Based on the subsequent flow modelling, the uncertainty related to the initial fracture aperture was high and, consequently, only relative displacements were used in the comparison (displacement difference from the zero-sensor position). The difference in the comparison is likely due to having earlier contact with the sharp surface undulations in the model and due to an imperfect material model without permanent deformation.

In the second modelling step, the deformed void space was used to model the water flow in the fracture and to predict flow rates with a varying normal load (blind predictions only with 1 MPa normal load) on the top rock part and an inlet and outlet pressure corresponding to the POST experiment (see the Task Description). The predicted flow rates with aperture distributions calculated using either of the contact models were significantly larger than the experimental results. The following factors were assumed to contribute the deviation, but they are not considered to explain it fully.

- 1) A contact offset was required to prevent geometrical and mesh overlap when the contact model was converted into a fluid flow model. Even if the deformation of the rock was modelled more precisely, the contact offset adds at least an error on the order of 0.1 ml/s to the predicted flow rates. The error does not account for the orders of magnitude difference in the predicted and experimental flow rates. The difference is more likely to originate from the following three problems. The error originating from the contact offset is, however, problematic especially for slow fracture flow rates as in the POST experiment, where the aperture between the two fractures is small.
- 2) The effect of the model precision inherited from the fracture surface scans on the flow rate was assessed. It was determined that the fracture scan precision of 0.035 mm also contributes from a threefold to a tenfold error when compared with the experimentally determined flow rates.

- 3) The provided experimental fracture surface data had some initial overlap (top surface overlapped the bottom surface) that had to be cut out of the model geometry to respect the initial measured placements of the top and bottom fracture surfaces. Such clipping removed the extra volume likely produced when opening the fracture (permanent deformation due to breaking of the rock) from the model and lowered the very high stress concentrations in the areas of the overlap, but at the cost of a more perfect, smooth contact between the rock parts. Such an increase in contact areas due to clipping were assumed to limit deformation of the void space elsewhere in the model when the rock parts were compressed together.
- 4) The numerical error, especially due to the fracture surface geometry interpolation, is a source of uncertainty for the model results. The effect of the interpolation error (or other numerical errors resulting from, for example, meshing) was not studied in detail.
- 5) The rock mechanical model was only elastic and lacked the ability to reproduce the likely breaking off parts of the rock during the normal compression or decompression. Consequently, the fracture aperture may have remained more open than in the experiment. Based on the LVDT data comparison, however, the trend of the displacement during compression was captured reasonably well.
- 6) In our model, the relative movement of the two fracture surfaces in x- and y-directions was limited, which could prevent interlocking of the two fracture surfaces in the lowest possible configuration. In future models, such movements could be allowed to obtain a better understanding of the process.

This report showed that contact modelling of complicated fracture surfaces is difficult to carry out. The modelling is also computationally intensive, slowing down iterations between different models. It also showed that the deformed aperture void space plays a significant role in the predicted flow rate and thus any modelling assumptions that would affect the resulting apertures should be well justified.

In addition to the modelling, a validation rank approach to complement the pragmatic validation idea by the Task Force was proposed. There, the validity rank of a model could be calculated based on the number of phenomena the model has been validated for, the number of validation-for-a-phenomenon exercises the model has passed, and the number of coupled validation exercises it has passed. The approach was tested for the modelling in the report. The outcome suggests that the approach should be further tested for other modelling and likely improved at least in the details.

Recommendations

It would be beneficial to carry out preliminary modelling in advance of any experiments such as the POST experiment. This way, a small enough measurement precision (for surface scanning) could be determined before the experiments to ensure that the fracture surface data sets are accurate enough to allow for an accurate prediction of flow rates. Such preliminary modelling could also indicate how influential small uncertainties in the experimental setups are, such as breaking of the rock that occurred during the rock part splitting. As small deviations in the predicted aperture have a significant effect on the predicted flow rate, a corresponding accuracy of the scanned surfaces should be ensured.

Another recommendation would be using smaller samples for the flow experiments. This way, the surface scan resolution could remain high without making the datasets impractical to use. With smaller datasets, model development would be faster, allowing for more time to adjust the models and, for example, perform sensitivity analyses.

Regarding the contact modelling approach in this report, it cannot be recommended for prediction of flow rates in experiments with very slow flow rates such as the POST experiment. The details of the deformed void space influence the flow rate significantly, and thus the rock-mechanical contact modelling has to be very accurate, which is likely not pragmatic. If permanent deformation models of the rock would be added to the linear elastic model in this study, the needed computational effort would be even higher and simulation times longer making the approach impractical. This, combined with the inherent problem with the contact offset, makes the approach impractical for sufficiently detailed fracture geometries even in centimetre scale for large datasets and fractures with small flow rates.

References

SKB's (Svensk Kärnbränslehantering AB) publications can be found at www.skb.com/publications.

Bartels R H, Beatty J C, Barsky B A, 1998. Hermite and Cubic Spline Interpolation. *Ch. 3 in An Introduction to Splines for Use in Computer Graphics and Geometric Modelling*. San Francisco, CA: Morgan Kaufmann.

Brady B H G, Brown E T, 1985. *Rock Mechanics For Underground Mining*. Goerge Allen & Unwin.

Chaboche J L, Feyel F, Monerie Y, 2001. Interface debonding models: a viscous regularization with limited rate dependency, *International Journal of Solids and Structures*, vol. 38, pp. 3127–3160.

COMSOL, 2022a. Comsol Documentation. Online, available at: <https://doc.comsol.com/6.1/docserver/#!/com.comsol.help.comsol/helpdesk/helpdesk.html>

COMSOL, 2022b. Structural Contact Modeling Guidelines. Online, available at: Structural Contact Modeling Guidelines - Knowledge Base (comsol.com)

Geological Survey of Finland, 1997. Interpretations of the Gravity Anomaly Map of Finland. *Geophysica*, 33(1).

Godio M, Jacobsson L, 2024. Experimental study on the hydromechanical behaviour of a natural unperturbed fracture under normal loading: Derivation of the equivalent hydraulic aperture and its digital reconstruction. RISE Report 2024:8. ISBN 978-91-89896-49-9. <http://urn.kb.se/resolve?urn=urn:nbn:se:ri:diva-71540>

IAEA, 2019. IAEA safety glossary: 2018 edition. International Atomic Energy Agency, Vienna.

Jacobsson L, Godio M, 2023. Measuring the hydraulic transmissivity of a rock joint under varying normal load. IOP Conference Series: Earth and Environmental Science, Volume 1124, Rock and Fracture Mechanics in Rock Engineering and Mining 11/09/2022 - 15/09/2022 Helsinki, Finland. DOI:10.1088/1755-1315/1124/1/012050.

Jones B, Nachtsheim C J, 2011. A class of three-level designs for definitive screening in the presence of second-order effects. *Journal of Quality Technology*, 43(1), 1–15.

Jones B, Nachtsheim C J, 2013. Definitive screening designs with added two-level categorical factors. *Journal of Quality Technology*, 45(2), 121–129.

Lanyon G W, Davy P, Dershowitz W S, Finsterle S, Gylling B, Hyman J D, Neretnieks I, Uchida M, 2021. Pragmatic Validation Approach for Geomechanics, Flow, and Transport Models in Fractured Rock Masses. Paper (DFNE 21-2369) presented at the 3rd International Discrete Fracture Network Engineering Conference, Virtual, June 2021.

Lennon E W, 2014. Thermophysical Properties of Water and Steam. In W. M. Haynes, D. R. Lide, & T. J. Bruno (Eds.), *CRC Handbook of Chemistry and Physics* (95th edition ed.). CRC Press.

Minitab, 2021. Interpret the key results for Analyze Definitive Screening Design. <https://support.minitab.com/en-us/minitab/20/help-and-how-to/statistical-modeling/doe/how-to/screening/analyze-screening-design/interpret-the-results/key-results/>

Can water pressure open the fracture in the POST experiment zero load case?

The moment and force balance of the top rock half is calculated below to estimate, if the water pressure in the POST experiment fracture could open the fracture.

Moment balance

The fracture can be opened by water pressure at the inlet side, if the moment due to water pressure with respect to the point $x=0$ (Figure A1) is greater than the moment due to the force compressing the top rock piece from above (due to the self-weight of the rock sample and loading plates as well as the additional load applied by the machine by the triaxial device).

The water pressure with respect to coordinate x is estimated to be linearly distributed such that

$$P(x) = \frac{P_{in} - P_{out}}{a}x + P_{out}$$

where P_{in} is the inlet pressure at $x = a$, P_{out} the outlet pressure at $x = 0$ and a the length of the fracture (that is the same as the width). The moment due to this is

$$M_{water} = \int_0^a P(x)x dx = \left[\frac{1}{3}P_{in} + \frac{1}{6}P_{out} \right] a^3.$$

The measured maximum values for the pressures in the zero load case are $P_{in} = 0.49$ bar and $P_{out} = 0.07$ bar. With these and $a = 200$ mm, the moment is 140 Nm.

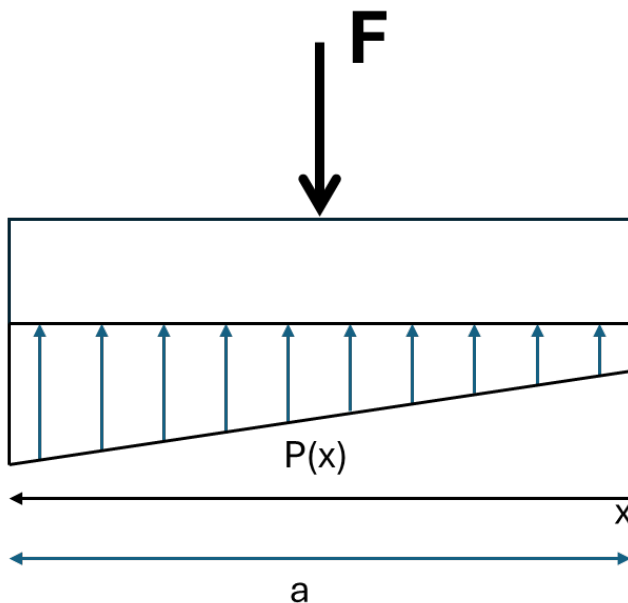


Figure A1. A schematic figure of force F compressing the top rock half from above and the water pressure $P(x)$ lifting the rock half.

Assuming pointwise force F at $x = 1/2a$ (or equal distribution of the load) from above, the moment due to it is

$$M_{tri} = F \frac{1}{2} a,$$

where F is the measured force. The best estimate for F in the zero load case is 0.63 kN. Consequently, the moment is 63 Nm.

Force balance

The top rock part can be lifted up by the water pressure, if the force due to water pressure is greater than the force compressing the top part from above. Assuming similar linear distribution of the water pressure as in the moment balance calculation, the force due to water pressure is

$$F_{\text{tri}} = \frac{1}{2}(P_{\text{in}} + P_{\text{out}})a^2.$$

With the same values as for the moment balance equation, the lifting force due to water pressure is 1,1 kN, which is twice the best estimate force compressing the top rock part from above.

Conclusions

Based on the moment and force balance calculations, the water pressure can lift and open the top rock part in the POST experiment in the zero load case. In fact, these calculations show that the top rock part should have been completely opened due to the water pressure and clearly seen in the measurements or even by eye. Since this was not the case, the top rock part was kept in place by the experiment setup (for example, no movement of the rock part allowed horizontally) or some phenomena or devices are not included in the best estimate value for the force compressing the rock parts together. In the loaded cases (with the forces above 20 kN and the respective moments above 2 kNm), the water pressure cannot move the rock parts.